XLIIIrd RENCONTRES DE MORIOND

Electroweak Interactions and Unified Theories

I I- Particle Searches, Supersymmetry, Theoretical issues

SUSY DARK MATTER

S. KRAML
LPSC, 53 av des Martyrs, 38026 Grenoble, France
email: sabine.kraml@lpsc.in2p3.fr

Collider searches for new physics and direct searches for dark matter are important topics at this conference. In this contribution, I discuss their potential synergy and complementarity by means of the minimal supersymmetric standard model with a neutralino dark matter candidate.

1 Introduction

Cosmological data ranging from the cosmic microwave background to rotation curves of spiral galaxies tell us that most of the mass in the Universe is provided by non-luminous, hence 'dark' matter [1,2,3]. More precisely, the recent measurements from WMAP [4] and SDSS [5] imply a (dominantly cold) dark matter density of $\Omega h^2 \simeq 0.1$ to an accuracy of about 10%.[a] The nature of this dark matter is one of the big open questions of present-day physics. Many lines of reasoning suggest, however, that it consists of a new weakly interacting massive particle, a so-called WIMP.

At the same time, we know that the Standard Model (SM) of particle physics, despite its tremendous success at energies up to ~ 100 GeV, is incomplete. In attempts to embed the SM in a more fundamental frame, theorists have come up with a wealth of Beyond the Standard Model (BSM) theories, which typically predict new particles and phenomena at the TeV energy scale. To probe this exciting new frontier is indeed the primary motivation to build the LHC! It is even more exciting that the lightest of these new BSM particles is often stable by virtue of a new discrete symmetry (introduced to match electroweak precision measurements and/or the non-observation of proton decay) and hence provides a natural dark matter candidate.

The dark matter candidates such put forth by particle physics are quite numerous [3] and contain, for example, the lightest supersymmetric particle in supersymmetry with R-parity con-

[a] The exact mean value and error depend on the data combination and number of parameters fitted, see Ref. [6].

Standard Model particles and fields		Supersymmetric partners			
		Interaction eigenstates		Mass eigenstates	
Symbol	Name	Symbol	Name	Symbol	Name
$q = d, c, b, u, s, t$	quark	$\tilde{q}_L$, $\tilde{q}_R$	squark	$\tilde{q}_1$, $\tilde{q}_2$	squark
$l = e, \mu, \tau$	lepton	$\tilde{l}_L$, $\tilde{l}_R$	slepton	$\tilde{l}_1$, $\tilde{l}_2$	slepton
$\nu = \nu_e, \nu_\mu, \nu_\tau$	neutrino	$\tilde{\nu}$	sneutrino	$\tilde{\nu}$	sneutrino
g	gluon	$\tilde{g}$	gluino	$\tilde{g}$	gluino
$W^\pm$	W-boson	$\tilde{W}^\pm$	wino	$\tilde{\chi}^\pm_{1,2}$	chargino
H^-	Higgs boson	$\tilde{H}_1^-$	higgsino		
H^+	Higgs boson	$\tilde{H}_2^+$	higgsino		
B	B-field	$\tilde{B}$	bino	$\tilde{\chi}^0_{1,2,3,4}$	neutralino
W^3	W^3-field	$\tilde{W}^3$	wino		
H_1^0	Higgs boson	$\tilde{H}_1^0$	higgsino		
H_2^0	Higgs boson	$\tilde{H}_2^0$	higgsino		
H_3^0	Higgs boson				

Table 1: Standard Model particles and their superpartners in the MSSM [3].

servation; the lightest Kaluza–Klein (KK) excitation in models with extra dimensions and KK-parity; the lightest T-odd state in little Higgs models with T-parity; etc. Note that all these possibilities are generally testable in collider experiments. This creates a strong interplay [7,8] between particle physics, astrophysics and cosmology, at both theoretical and experimental levels.

2 Supersymmetry

Of the existing BSM theories, supersymmetry (SUSY) [9] is arguably the best motivated one. SUSY is a symmetry between fermions and bosons. A SUSY generator Q changes a fermion into a boson and vice versa:

$$Q|\text{fermion}\rangle = |\text{boson}\rangle\,, \quad Q|\text{boson}\rangle = |\text{fermion}\rangle\,. \tag{1}$$

This is an extension of space-time to include anti-commuting coordinates $x^\mu \to (x^\mu, \theta^\alpha)$ with $\{\theta^\alpha, \theta^\beta\} = \varepsilon^{\alpha\beta}$, combining the relativistic 'external' symmetries (such as Lorentz invariance) with the 'internal' symmetries of a field, such as weak isospin. It is in fact the unique(!) extension of the Poincaré algebra (the algebra of space-time translations, rotations and boosts).

From the phenomenological point of view, SUSY predicts a partner particle, a so-called 'superpartner' or 'sparticle', for every SM state.[b] The particle content of the Minimal Supersymmetric Standard Model (MSSM), is given in Table 2. In its local gauge theory version, SUSY also includes spin-2 and spin-3/2 states, the graviton and its superpartner the gravitino and is hence potentially capable of connecting gravity with the other interactions (so-called supergravity or short SUGRA). A few more things are important to observe:

i) SUSY must be a broken symmetry, else SM particles and their superpartners would have equal mass. In order to still solve the hierarchy problem of the SM (i.e. to stabilize the electroweak scale against quadratically divergent radiative corrections) and to achieve gauge-coupling unification, one expects the superpartners to have masses of $m \leq \mathcal{O}(1)$ TeV.

ii) After electroweak symmetry breaking, we are left with three neutral Higgs bosons: two scalars h, H and one pseudoscalar A. Moreover, sparticles with the same SU(3)×U(1) quantum numbers mix, c.f. Table 2. In particular, the bino, wino and neutral higgsinos mix to mass eigenstates called neutralinos $\tilde{\chi}^0_{1,\ldots,4}$ (with $\tilde{\chi}^0_1$ the lightest one by definition).

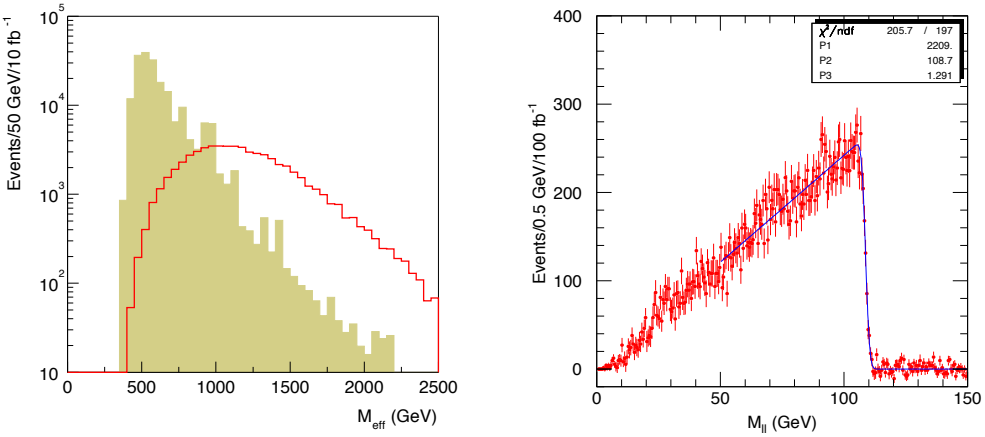

Figure 1: Left: $M_{\rm eff}$ distribution for a SUGRA point with gluino and squark masses of about 700 GeV (histogram) and Standard Model background (shaded) after cuts. Right: Di-lepton invariant-mass distribution from $\tilde{\chi}_2^0 \to \tilde{l}^{\pm} l^{\mp} \to l^+ l^- \tilde{\chi}_1^0$ decays. From [15].

iii) If SUSY comes with a new conserved parity, so-called R-parity, under which SM particles are even and SUSY particles are odd, the lightest supersymmetric particle (LSP) is stable. in this case it has to be electrically and colour neutral and constitutes a natural dark matter candidate.

In the following I concentrate on the MSSM with a neutralino LSP. For gravitino dark matter, which has a quite different phenomenology, I refer to the contribution by F. Steffen in these proceedings. Sneutrinos in extensions of the MSSM are discussed by C. Arina in the YSF.

3 Collider searches

If low-scale supersymmetry is realized in Nature, experiments at the LHC have excellent prospects to discover it [10,11,12]. In particular, squarks and gluinos should be copiously produced at the LHC through the QCD interaction, with cross sections of $\mathcal{O}(1)$ pb for masses around 1 TeV.

This is followed by (multi-step) decays into lighter sparticles. Squarks decay into gluinos plus jets, $\tilde{q} \to q\tilde{g}$, if kinematically allowed, or into charginos/neutralinos plus jets, $\tilde{q}_L \to q'\tilde{\chi}_i^{\pm}$, $q\tilde{\chi}_j^0$ and $\tilde{q}_R \to q\tilde{\chi}_j^0$ $(i = 1, 2;\ j = 1, ..., 4)$. Gluinos always decay into squarks, either in the two-body mode $\tilde{g} \to q\tilde{q}$ if kinematically open, or else $\tilde{g} \to q\bar{q}'\tilde{\chi}_i^{\pm}$, $q\bar{q}\tilde{\chi}_j^0$ via an off-shell squark. The charginos $\tilde{\chi}_{1,2}^{\pm}$ and neutralinos $\tilde{\chi}_{2,3,4}^0$ decay further, e.g. $\tilde{\chi}_i^{\pm} \to W^{\pm}\tilde{\chi}_j^0$ or $\tilde{\chi}_k^0 \to Z\tilde{\chi}_j^0$, until the LSP $\tilde{\chi}_1^0$ is reached. The LSP, being stable and neutral, escapes undetected.

SUSY events are hence characterized by multiple hard jets, maybe accompanied by leptons, plus large missing transverse energy $E_T^{\rm miss}$. The significance of such a signal over the SM background is illustrated in the left plot in Fig. 1, which shows the number of events as a function of the 'effective mass' computed from the missing energy and the momenta of the hardest jets, $M_{\rm eff} = E_T^{\rm miss} + \sum p_T^{\rm jets}$. Note that the y-axis is log-scale! The $M_{\rm eff}$ distribution also provides a first estimate of the gluino/squark mass scale.

In certain scenarios and/or with high enough statistics, electroweak production of charginos and neutralinos, e.g., $pp \to \tilde{\chi}_1^{\pm}\tilde{\chi}_1^{\mp}$, $\tilde{\chi}_1^{\pm}\tilde{\chi}_2^0$, can also be important. The latter process can lead to the goldplated tri-lepton signal, which is also searched for at the Tevatron [13]. Moreover, for slepton masses up to 300 GeV, slepton-pair production can lead to detectable di-lepton signals.

The discovery of SUSY particles will be followed by detailed measurements of their masses and decay properties. Since the LSP escapes as missing energy, no mass peaks can be reconstructed. Instead, mass measurements exploit kinematic distributions in cascade decays [14,15]. For

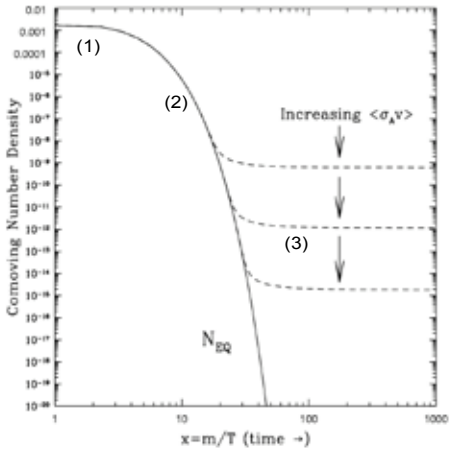

Figure 2: The cosmological evolution of a thermal relic's comoving number density, from [1]. The full line is the equilibrium abundance; the dashed lines are the actual abundance after freeze-out. As the annihilation cross section $\langle\sigma_A v\rangle$ is increased, the WIMP stays in equilibrium longer, leading to a smaller relic density.

instance, the invariant-mass distribution of the leptons stemming from the chain $\tilde{\chi}_2^0 \to l^{\pm}\tilde{l}^{\mp} \to l^+l^-\tilde{\chi}_1^0$ has a triangular shape with a sharp endpoint at $M_{ll}^{\max} = [(m^2_{\tilde{\chi}_2^0} - m^2_{\tilde{l}})(m^2_{\tilde{l}} - m^2_{\tilde{\chi}_1^0})/m^2_{\tilde{l}}\,]^{1/2}$, which can be measured very precisely, see the right plot in Fig. 1. If the leptons come from the three-body decay $\tilde{\chi}_2^0 \to l^+l^-\tilde{\chi}_1^0$, M_{ll} has a different shape and an endpoint at $m_{\tilde{\chi}_2^0} - m_{\tilde{\chi}_1^0}$. Additional distributions can be constructed involving jets stemming from gluino and squark decays. This way the masses of the sparticles appearing in the decay chains can be reconstructed.

Let us finally come back to the dark matter question. The alert reader will have noticed that because of R-parity sparticles are produced in even numbers, and every sparticle decay terminates in the LSP. As a consequence, each SUSY event contains two LSPs. Moreover, if squarks and gluinos weigh about 1 TeV, we expect of the order of 100 events/day —at low luminosity. The LHC may hence well turn out as a dark matter factory, where the nature and properties of dark matter candidates may be studied in a controlled environment.

Typical precisions at the LHC are $\mathcal{O}(10\%)$. Much higher precisions at the percent to permil level might be achieved at an International e^+e^- Linear Collider (ILC) [16]. The determination of neutralino dark matter properties at LHC and ILC has been analyzed, e.g., in [17].

4 Relic density

The standard cosmological scenario assumes that the dark matter particle, let us call it χ, is a thermal relic of the Big Bang as illustrated in Fig. 2: When the early Universe was dense and hot, $T \gg m_\chi$, χ was in thermal equilibrium; annihilation of χ and $\bar{\chi}$ into lighter particles, $\chi\bar{\chi} \to l\bar{l}$, and the inverse process $l\bar{l} \to \chi\bar{\chi}$ proceeded with equal rates. As the Universe expanded and cooled to a temperature $T < m_\chi$, the number density of χ dropped exponentially, $n_\chi \sim e^{-m_\chi/T}$. Eventually the temperature became too low for the annihilation to keep up with the expansion rate and χ 'froze out' with the cosmological abundance observed today.

The time evolution of the number density $n_\chi(t)$ is described by the Boltzman equation,

$$\mathrm{d}n_\chi/\mathrm{d}t + 3Hn_\chi = -\langle\sigma_A v\rangle\,[(n_\chi)^2 - (n_\chi^{\mathrm{eq}})^2]\,, \qquad (2)$$

where H is the Hubble expansion rate, n_χ^{eq} is the equilibrium number density, and $\langle\sigma_A v\rangle$ is the thermally averaged cross section times the relative velocity of the annihilating particles. The relic density today turns out to be inversely proportional to the annihilation cross section,

$\Omega_\chi h^2 \propto 1/\langle\sigma_A v\rangle$. Note that $\langle\sigma_A v\rangle$ includes a sum over all possible annihilation channels for the LSP. These are annihilation into gauge boson pairs through t-channel chargino and neutralino exchange, and annihilation into fermion pairs through t-channel sfermion exchange and s-channel Z/Higgs exchange. Moreover, co-annihilation channels involving sparticles that are close in mass to the LSP have to be taken into account. For details of the calculation, see [2,18].

The relic density of the LSP hence depends on all the MSSM masses and couplings that enter the different annihilation/co-annihilation channels. On the one hand, this is often used to severely constrain SUSY models by demanding that the relic density of the LSP falls within the WMAP–SDSS range (see the YSF contribution by S. Sekmen for an example). On the other hand, if the masses and couplings of SUSY particles are measured precisely enough, $\Omega_\chi h^2$ can be computed and compared to the cosmologically observed value.

Here notice that the standard picture heavily relies on two assumptions: i) that the initial temperature after inflation has been high enough to fully thermalize the LSP and ii) that the entropy per comoving volume has been constant below the freeze-out temperature. In non-standard scenarios with low reheat temperature and/or late entropy production, the relic density can be quite different from the value in the standard scenario. A precise determination of the LSP annihilation cross section from collider experiments, together with a confirmation that the LSP is indeed the cold dark matter through direct detection (see next section), will hence allow to probe these asumptions [19], i.e. probe the evolution of the early universe up to the freeze-out temperature $T_f \sim m_\chi/20$.

5 Direct detection

Experiments such as CDMS[20], XENON[21], ZEPLIN[22], EDELWEISS[23], CRESST[24], KIMS[25] and COUPP [26] aim at detecting WIMPs through their elastic scattering with nuclei. The current experimental limits and projected sensitivities are shown in Fig. 3, together with predictions from various MSSM scenarios. Principally one distinguishes two classes, spin-dependent and spin-independent interactions. On the partonic level, WIMP interactions with quarks and gluons in the nucleons contribute.

In the case of neutralino dark matter, the scattering off quarks can occur through t-channel exchange of Z or CP-even Higgs bosons, or s-channel exchange of squarks:

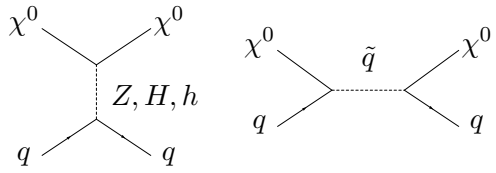

The diagrams with Z and squark exchange contribute to the axial-vector (spin) interaction, $\mathcal{L} \sim \bar{\chi}\gamma^\mu\gamma^5\chi\bar{q}\gamma_\mu\gamma_5 q$. The Higgs and squark exchange diagrams contribute to the scalar (spin-independent) interaction, $\mathcal{L} \sim \bar{\chi}\chi\bar{q}q$. The neutralino interaction with gluons proceeds through quark and squark loops and contributes to the spin-independent cross section. See [2,27] for details. Note that since the neutralino is a Majorana particle, there is no vector interaction of the form $\mathcal{L} \sim \bar{\chi}\gamma^\mu\chi\bar{q}\gamma_\mu q$.

The effective neutralino–nucleon coupling hence depends on the neutralino mass and decomposition (i.e. the bino/wino/higgsino content) as well as on the Higgs and squark masses and couplings. Again, if the supersymmetric spectrum is known from collider experiments, the scattering cross section can be predicted.[c] A word of caution is, however, in order here because the strange content of the nucleon is not known well; this induces a considerable uncertainty [29] in the neutralino–nucleon cross section, in particular if Higgs exchange dominates. Finally, the

[c] This cross section also determines the rate at which neutralinos would accrete in the Earth and Sun.

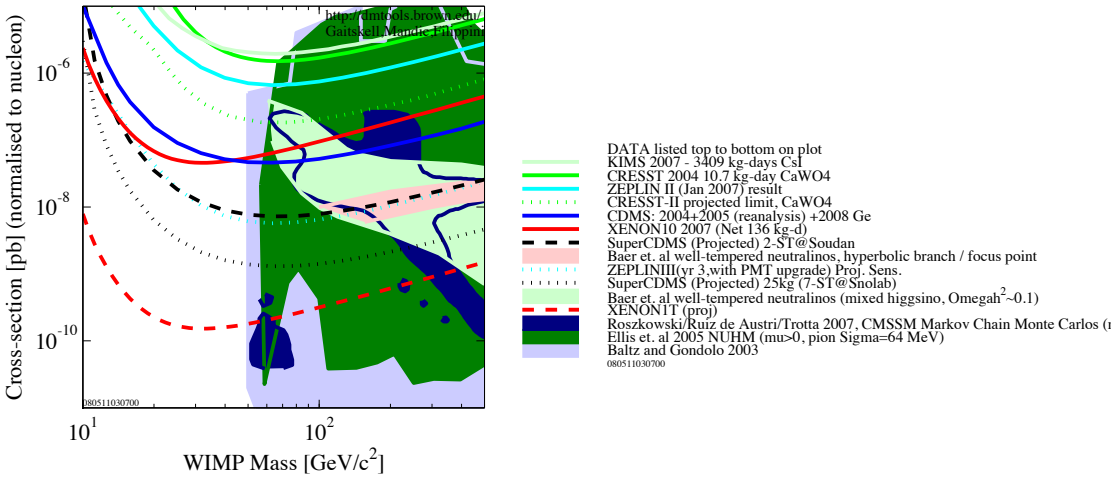

Figure 3: Direct detection of WIMP dark matter: current experimental limits and projected sensitivities, together with various SUSY model predictions; generated with `DMTOOLS` [28].

neutralino–nucleon cross sections $\sigma_{\chi n}$ and $\sigma_{\chi p}$ have to be translated to the neutralino–nucleus scattering cross section $\sigma_{\chi N}$ applying nuclear form factors.

The actual direct-detection rate depends, moreover, on the local dark matter density ρ_χ and the velocity distribution $f(v)$. Roughly speaking, the rate of events per day and per kg of detector material is $R \sim \rho_\chi \sigma_{\chi N} \langle v \rangle / (m_\chi m_N)$, with m_N the target nucleus mass and $\langle v \rangle$ the average velocity of χ relative to the target. Typical estimates are $\rho_\chi = 0.22 - 0.73$ GeV/cm^3 and $\langle v \rangle = 230 \pm 20$ km/s. If m_χ and $\sigma_{\chi N}$ are known with good precision, the local density and velocity distribution can be tested.

At this point, let me stress the importance of direct detection for another reason: Although collider experiments may identify a dark matter candidate and precisely measure its properties, they will not be able to distinguish a cosmologically stable from a very long-lived but unstable particle. Therefore validation of the collider signal through direct detection is essential. The key to this is the WIMP mass, which may be determined [30,31] in direct-detection experiments through the distribution of the recoil energy, $E_R \propto 2v^2 m_N / (1 + m_N/m_\chi)^2$. Note that E_R is sensitive to small m_χ but becomes almost constant for $m_\chi \gg m_N$. Note also the velocity dependence, which is source of considerable uncertainty in a single experiment. This may be evaded by using multiple targets [31]. Precisions are, however, still poor for $m_\chi \gg m_N$.

6 Conclusions

For conclusions, let me cite G. F. Giudice in "Theories for the Fermi scale" [32]: *It is impossible to overestimate the importance of discovering dark matter at the LHC. Such a discovery will imply a revision of the SM, it will strenghten the connection between particle physics, cosmology and astrophysics, and it will enormously enlarge our understanding of the present and past universe.*

So be prepared for exciting times at future Moriond meetings.

Acknowledgments

I wish to thank the organisers for creating a remarkably pleasant and inspiring atmosphere. Fruitful discussions with other participants are also gratefully acknowledged.

References

1. E. W. Kolb and M. S. Turner, *The Early universe*, Front. Phys. **69** (1990) 1.
2. G. Jungman, M. Kamionkowski and K. Griest, Phys. Rept. **267** (1996) 195, hep-ph/9506380.
3. G. Bertone, D. Hooper and J. Silk, Phys. Rept. **405** (2005) 279, hep-ph/0404175.
4. D. N. Spergel *et al.*, Astrophys. J. Suppl. **170** (2007) 377, astro-ph/0603449; E. Komatsu *et al.*, arXiv:0803.0547 [astro-ph].
5. M. Tegmark *et al.*, Phys. Rev. **D69** (2004) 103501, astro-ph/0310723.
6. J. Hamann, S. Hannestad, M. S. Sloth and Y. Y. Y. Wong, Phys. Rev. D **75** (2007) 023522, astro-ph/0611582.
7. D. Hooper and E. A. Baltz, arXiv:0802.0702 [hep-ph].
8. H. Baer and X. Tata, arXiv:0805.1905 [hep-ph].
9. See e.g., H. Baer and X. Tata, *Weak scale supersymmetry: From superfields to scattering events*, Cambridge University Press (2006).
10. ATLAS Collaboration, *ATLAS Detector and Physics Performance: Technical Design Report*, vol. 2, ATLAS-TDR-15, CERN-LHCC-99-15 (1999).
11. CMS Collaboration, *CMS Physics: Technical Design Report, Volume 2: Physics Performance*, CMS-TDR-8.2, CERN-LHCC-2006-021 (2006).
12. S. Tsuno, these proceedings.
13. S. Dube, these proceedings.
14. I. Hinchliffe, F. E. Paige, M. D. Shapiro, J. Soderqvist and W. Yao, Phys. Rev. D **55** (1997) 5520, hep-ph/9610544.
15. H. Bachacou, I. Hinchliffe and F. E. Paige, Phys. Rev. D **62** (2000) 015009, hep-ph/9907518.
16. G. Weiglein *et al.*, Phys. Rept. **426** (2006) 47, hep-ph/0410364; `http://www.linearcollider.org`.
17. E. A. Baltz, M. Battaglia, M. E. Peskin and T. Wizansky, Phys. Rev. D **74** (2006) 103521, hep-ph/0602187.
18. M. Drees and M. M. Nojiri, Phys. Rev. D **47** (1993) 376, hep-ph/9207234.
19. M. Drees, H. Iminniyaz and M. Kakizaki, Phys. Rev. D **76** (2007) 103524, arXiv:0704.1590 [hep-ph], and references therein.
20. Z. Ahmed *et al.*, arXiv:0802.3530 [astro-ph]; D. S. Akerib *et al.*, Phys. Rev. D **73** (2006) 011102, astro-ph/0509269.
21. J. Angle *et al.*, Phys. Rev. Lett. **100** (2008) 021303, arXiv:0706.0039 [astro-ph]; R. Santorelli, these proceedings.
22. G. J. Alner *et al.*, Astropart. Phys. **28** (2007) 287, astro-ph/0701858.
23. V. Sanglard *et al.*, Phys. Rev. D **71** (2005) 122002, astro-ph/0503265.
24. G. Angloher *et al.*, Astropart. Phys. **23** (2005) 325 , astro-ph/0408006; R. F. Lang, these proceedings.
25. H. S. Lee. *et al.*, Phys. Rev. Lett. **99** (2007) 091301, arXiv:0704.0423 [astro-ph]; S. K. Kim, these proceedings.
26. W. J. Bolte *et al.*, J. Phys. Conf. Ser. **39** (2006) 126; M. Szydagis, these proceedings.
27. M. Drees and M. Nojiri, Phys. Rev. D **48** (1993) 3483 [arXiv:hep-ph/9307208].
28. R. Gaitskell, V. Mandic and J. Filippini, `http://dmtools.berkeley.edu/limitplots/`
29. J. Ellis, K. A. Olive and C. Savage, Phys. Rev. D **77** (2008) 065026, arXiv:0801.3656 [hep-ph]; G. Belanger, F. Boudjema, A. Pukhov and A. Semenov, arXiv:0803.2360 [hep-ph].
30. A. M. Green, JCAP **0708** (2007) 022, hep-ph/0703217; arXiv:0805.1704 [hep-ph].
31. M. Drees and C. L. Shan, arXiv:0803.4477 [hep-ph].
32. G. F. Giudice, arXiv:0710.3294 [hep-ph].

MODEL INDEPENDENT SEARCHES IN EP COLLISIONS

E. SAUVAN
On behalf of the H1 and ZEUS Collaborations
CPPM, IN2P3-CNRS et Université de la Méditerranée,
163 Av. de Luminy, F-13288 Marseille, France.

The high energy program of the HERA collider ended in March 2007. In total the H1 and ZEUS experiments collected an integrated luminosity of about 1 fb^{-1}. Recent results of model independent searches for new physics from both experiments are presented. Specifically, studies of the events with an isolated lepton and missing transverse momentum and multi-lepton topologies, where H1 and ZEUS data are combined, and a general signature based search are discussed.

1 Introduction

At HERA electrons (or positrons) collide with protons at a centre-of-mass energy of $\sqrt{s} \simeq 320$ GeV. During the two running periods of HERA from 1994 to 2000 and from 2003 to 2007, respectively, the H1 and ZEUS experiments have each recorded ~ 0.5 fb^{-1} of data in total, shared between e^+p and e^-p collision modes. These high energy electron-proton interactions provide a testing ground for the Standard Model (SM) complementary to e^+e^- and $p\bar{p}$ scattering studied at other colliders, giving access to rare processes with cross sections below 1 pb. They are therefore used to pursue a rich variety of searches for new phenomena. Among them, signature based searches look for differences in precise comparisons between data and SM expectations in different event topologies. As an advantage, such model independent analyses do not depend on any a priori definition of expected signatures for exotic phenomena. Following this approach, final states corresponding to rare SM processes such as real W boson or lepton pair production are investigated. A general scan at high transverse momenta (P_T) of all possible final states is also performed by H1.

2 Events with high P_T isolated leptons

The production of W bosons in ep collisions at HERA has a cross-section of about 1 pb. The leptonic decay of the W leads to events with an isolated high transverse momentum lepton (electron, muon or tau) and missing total transverse momentum. Of particular interest are events with a hadronic system of large transverse momentum (P_T^X). An abnormally large rate of high P_T^X events is observed by the H1 experiment [1,2] in the electron and muon channels. In the analysis of all HERA I and HERA II data sets, which amounts to a total luminosity of 478 pb^{-1}, 24 events are observed at $P_T^X > 25$ GeV for a SM expectation of 15.8 ± 2.5. Amongst them only 3 events are observed in e^-p collisions, in agreement with the SM expectation of 6.9 ± 1.0, while 21 events are observed in the e^+p data for an expectation of 8.9 ± 1.5 (see table 1).

Table 1: Comparison of the number of isolated lepton (electron or muon) events observed for $P_T^X > 25$ GeV by H1 and ZEUS experiments with SM predictions.

$P_T^X > 25$ GeV			Electron obs./exp.	Muon obs./exp.	Combined obs./exp.
H1	e^-p	184 pb^{-1}	3 / 3.8 ± 0.6	0 / 3.1 ± 0.5	3 / 6.9 ± 1.0
ZEUS	e^-p	206 pb^{-1}	3 / 3.2 ± 0.6	2 / 2.4 ± 0.4	6 / 5.6 ± 1.0
H1	e^+p	294 pb^{-1}	11 / 4.7 ± 0.9	10 / 4.2 ± 0.7	21 / 8.9 ± 1.5
ZEUS	e^+p	286 pb^{-1}	3 / 3.9 ± 0.6	3 / 3.6 ± 0.5	6 / 7.5 ± 1.1

The ZEUS experiment has carried out a similar analysis using 492 pb^{-1} of 1996–2007 data [3]. The results are also shown in table 1. At $P_T^X > 25$ GeV the number of data events observed by ZEUS is in agreement with the SM expectation in both e^+p and e^-p collisions. A detailed comparison between efficiencies of the H1 and ZEUS detectors for the W signal was performed. Both efficiencies are comparable in the central region. While H1 detection region extends to lower polar angle than ZEUS, most of the high P_T^X events observed by H1 are within the range of the ZEUS acceptance.

The data samples of the H1 and ZEUS experiments have been used for a combined analysis performed in a common phase space [4]. The combined data set corresponds to a total integrated luminosity of 0.97 fb^{-1}. A total of 87 events containing an isolated electron or muon and missing transverse momentum are observed in the data, compared to a SM expectation of 92.7 ± 11.2. At $P_T^X > 25$ GeV, a total of 29 events are observed compared to a SM prediction of 25.3 ± 3.2. In this kinematic region, 23 events are observed in the e^+p data compared to a SM prediction of 14.6 ± 1.9. The observations in the e^+p and e^-p data sets are exemplified in figure 1 where the P_T^X distributions of both data sets are displayed.

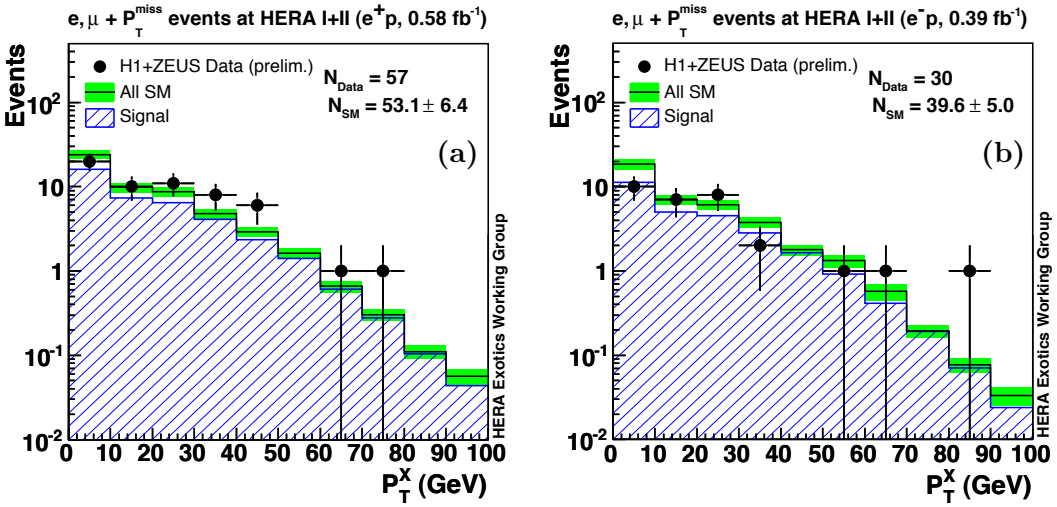

Figure 1: Hadronic transverse momentum distribution of isolated lepton events observed by H1 and ZEUS in e^+p (a) and e^-p (b) data samples. The total SM expectation is represented by the open histograms and the contribution from W production by the hatched histogram.

The analysis of the tau decay channel is also performed by H1 [5] on all HERA data with a total luminosity of 471 pb^{-1}. In this channel, the separation of the W signal from other SM processes is more difficult and the purity and efficiency are lower than for the e and μ channels. In total, 20 data events are observed compared to a SM expectation of 19.5 ± 3.2. One of the data events has P_T^X above 25 GeV, compared to a SM expectation of 0.99 ± 0.13. An older

analysis of the tau channel performed by the ZEUS Collaboration [6] on HERA I data reported an observation of two data events with $P_T^X > 25$ GeV, compared to a SM expectation of 0.2 ± 0.05.

3 Multi-lepton events

The main production mechanism for multi-lepton events is photon-photon collisions. All event topologies with high transverse momentum electrons and muons have been investigated by the H1 experiment [7] using a total luminosity of 459 pb^{-1}. The measured yields of di-lepton and tri-lepton events are in good agreement with the SM prediction, except in the tail of the distribution of the scalar sum of transverse momenta of the leptons ($\sum P_T$). In e^+p collisions, 4 data events with at least two high P_T leptons are observed with $\sum P_T > 100$ GeV compared to a SM prediction of 1.2 ± 0.2. No such events are observed in e^-p collisions for a similar SM expectation of 0.8 ± 0.2.

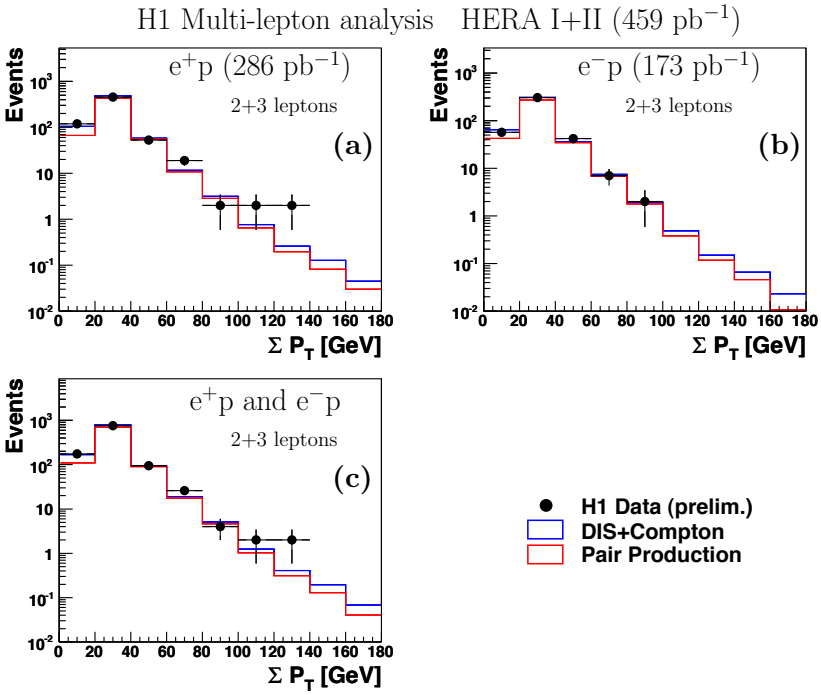

Figure 2: Distribution of the scalar sum of the transverse momenta of leptons compared to expectations separately for events recorded by H1 in e^+p (a) and e^-p (b) collisions and for all H1 data (c).

The analysis of di-electron ($2e$) and tri-electron ($3e$) topologies is also carried out by ZEUS using 478 pb^{-1} of data [8]. Two data events with an electron pair invariant mass above 100 GeV are observed in each $2e$ and $3e$ channel. These observations are in good agreement with the corresponding SM expectations of 1.9 ± 0.2 and 1.0 ± 0.1 in the $2e$ and $3e$ channels, respectively.

Analyses of the $2e$ and $3e$ topologies from the H1 and ZEUS experiments have been combined in a common phase space [9]. The total integrated luminosity amounts to 0.94 fb^{-1}. The measured event yields of di-electron and tri-electron events are in good agreement with the SM predictions. The distribution of the invariant mass M_{12} of the two highest P_T electrons in $2e$ and $3e$ channels is presented in figure 3. In the $2e$ ($3e$) channel, 5 (4) events with an invariant mass $M_{12} > 100$ GeV are observed compared to a SM expectation of 3.4 ± 0.4 (1.8 ± 0.2). Combining the two channels, six events are observed with $\sum P_T > 100$ GeV, compared to a SM expectation of 3.0 ± 0.3. Five of those events are observed in e^+p collisions where the SM expectation is of 1.8 ± 0.2, whereas one event is observed in e^-p data for a SM prediction of 1.2 ± 0.1.

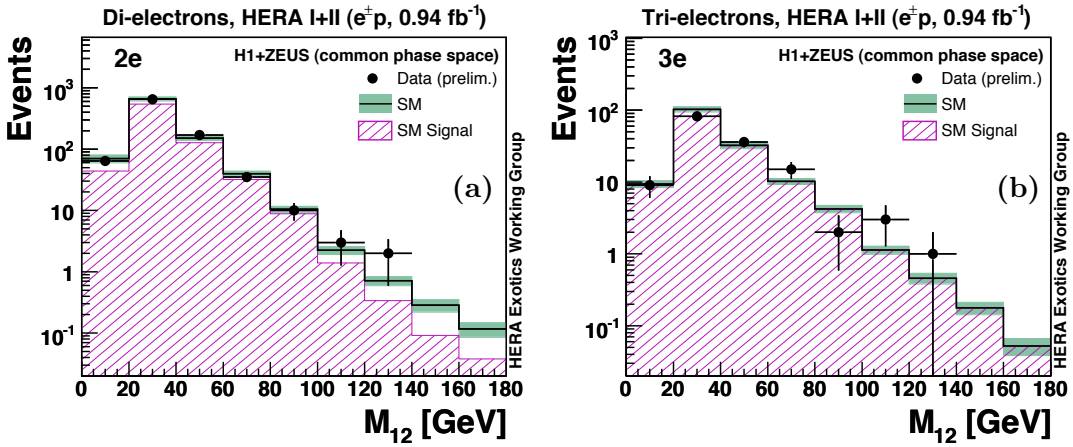

Figure 3: Distribution of the invariant mass M_{12} of the two highest P_T electrons of di-electron (a) and tri-electron (b) events observed by H1 and ZEUS in $e^{\pm}p$ data. The points correspond to the observed data events and the open histogram to the SM expectation. The total error on the SM expectation is given by the shaded band. The component of the SM expectation arising from lepton pair production is given by the hatched histogram.

4 A general search for new phenomena

A broad range signature based search has been developed by the H1 Collaboration on HERA I data [10]. All final states containing at least two objects (e, μ, j, γ, ν) with $P_T > 20$ GeV in the polar angle range $10^\circ < \theta < 140^\circ$ are now also investigated in all HERA II data [11]. The observed and predicted event yields in each channel are presented in figure 4(a) and (b) for e^+p and e^-p collisions, respectively. The good agreement observed between data and SM prediction demonstrates the good understanding of the detector and of the contributions of the SM backgrounds.

A systematic scan of the distributions of the scalar sum of transverse momenta $\sum P_T$ and of the invariant mass M_{all} of all objects is performed in each channel to look for regions of largest deviations from the SM. In order to quantify the level of agreement between the data and the SM expectation and to identify regions of possible deviations, the search algorithm developed in reference [10] is used. All possible regions in the histograms of $\sum P_T$ and M_{all} distributions are considered. A statistical estimator p is defined to judge which region is of most interest. This estimator is derived from the convolution of the Poisson probability density function (pdf) to account for statistical errors with a Gaussian pdf to include the effect of non negligible systematic uncertainties [10]. The value of p gives an estimate of the probability of a fluctuation of the SM expectation upwards (downwards) to at least (at most) the observed number of data events in the region considered. The region of greatest deviation is the region having the smallest p-value, $p_{\min}$. The fact that the deviation could have occured at any point in the distribution is taken into account by calculating the probability $\hat{P}$ to observe a deviation with a p-value $p_{\min}$ at any position in the distribution. This $\hat{P}$ is a measure of the statistical significance of the deviation observed in the data. The event class of most interest for a search is the one with the smallest $\hat{P}$ value.

The overall degree of agreement with the SM can further be quantified by taking into account the large number of event classes studied in this analysis. Among all studied classes there is some chance that small $\hat{P}$ values occur. This probability can be calculated with MC experiments. A MC experiment is defined as a set of hypothetical data histograms following the SM expectation with an integrated luminosity equal to the amount of data recorded. The complete search algorithm and statistical analysis are applied to the MC experiments analogously as to the data. The expectation for the $\hat{P}$ values observed in the data is then given by the distribution of $\hat{P}^{SM}$ values obtained from all MC experiments.

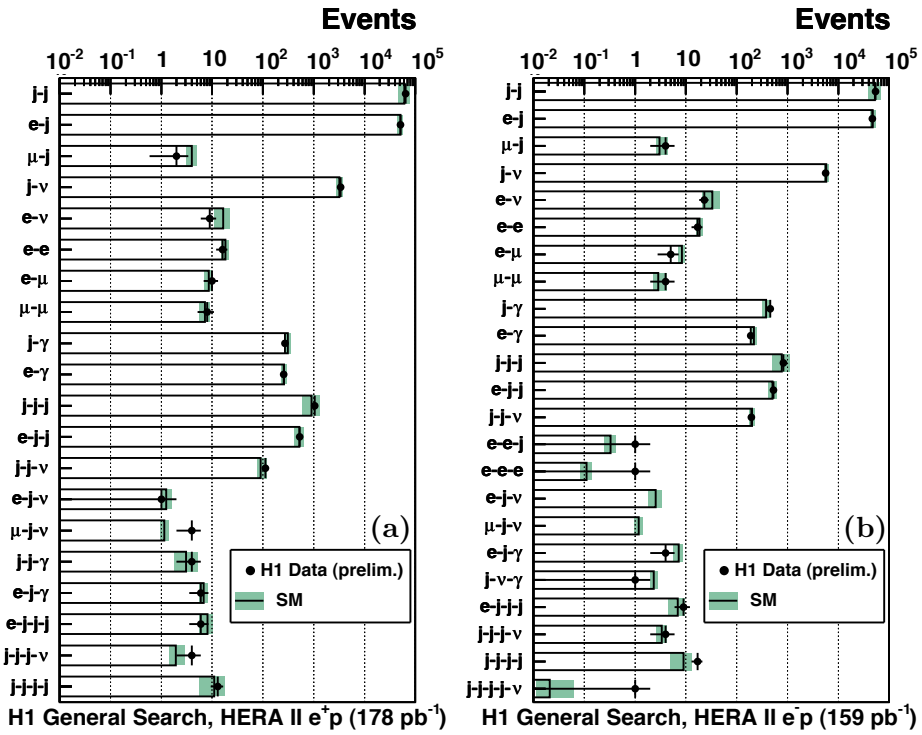

Figure 4: The data and the SM expectation in event classes investigated by the H1 general search. Only channels with observed data events or a SM expectation greater than one event are displayed. The results are presented separately for e^+p (a) and e^-p (b) collision modes.

The $\hat{P}$ values observed in the real data in all event classes are compared in figure 5 to the distribution of $\hat{P}^{SM}$ expected from MC experiments. The comparison is presented for the scans of the $\sum P_T$ distributions. Due to the uncertainties of the SM prediction in the *j-j-j-j* and *j-j-j-j-ν* event classes at highest M_{all} and $\sum P_T$ (see reference [10]), where data events are observed, no reliable $\hat{P}$ values can be calculated for these classes. These event classes are not considered to search for deviations from the SM in this extreme kinematic domain. All $\hat{P}$ values range from 0.01 to 0.99, corresponding to event classes where no significant discrepancy between data and the SM expectation is observed. These results are in agreement with the expectation from MC experiments. The most significant deviation from SM predictions is observed in the *μ-j-ν* event class in e^+p collisions with a value of $-\log_{10}\hat{P}$ equal to 1.7. In the previous H1 analysis [10] based on HERA I data, which is dominated by e^+p collisions, the largest deviation was also found in this event class, with $-\log_{10}\hat{P} = 3$.

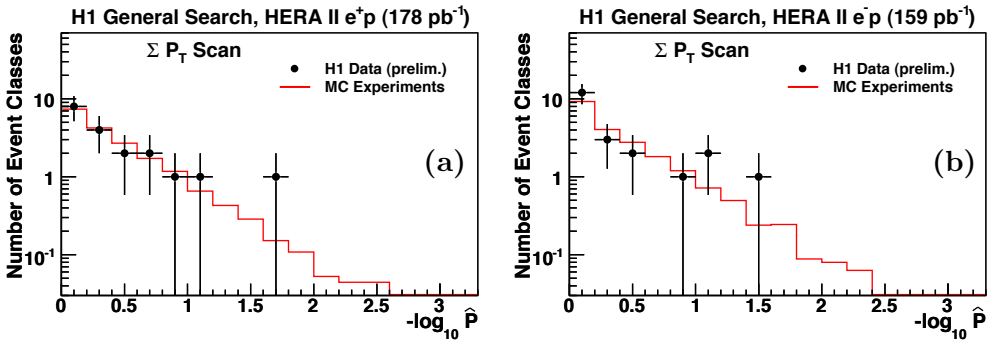

Figure 5: The $-\log_{10}\hat{P}$ values for the data event classes and the expected distribution from MC experiments as derived by investigating the $\sum P_T$ distributions in e^+p (a) and e^-p (b) data.

5 Conclusions

The recent results of model independent searches for new physics performed at the HERA ep collider have been presented. All analyses fully exploit the complete high energy data sample, which amounts to ~ 0.5 fb^{-1} per experiment. No convincing evidence for the existence of new phenomena beyond the Standard Model has been observed. Among all event topologies investigated, the largest deviation to the SM expectation is observed by the H1 experiment for isolated lepton events in e^+p collisions. After having analysed all data recorded by H1, this deviation corresponds to a 3 σ excess of atypical W-like events. This deviation is not confirmed by the ZEUS experiment.

References

1. V. Andreev *et al.* [H1 Collaboration], Phys. Lett. B **561** (2003) 241 [hep-ex/0301030].
2. H1 Collaboration, contributed paper to EPS-HEP07, H1prelim-07-063, available at http://www-h1.desy.de/h1/www/publications/htmlsplit/H1prelim-07-063.long.html
3. ZEUS Collaboration, contributed paper to EPS-HEP07, ZEUS-prel-07-021, available at http://www-zeus.desy.de/~ferrando/public_prel/eps07/
4. H1 and ZEUS Collaborations, contributed paper to EPS-HEP07, H1prelim-07-162, ZEUS-prel-07-029, available at http://www-h1.desy.de/h1/www/publications/htmlsplit/H1prelim-07-162.long.html
5. H1 Collaboration, contributed paper to EPS-HEP07, H1prelim-07-064, available at http://www-h1.desy.de/h1/www/publications/htmlsplit/H1prelim-07-064.long.html
6. S. Chekanov *et al.* [ZEUS Collaboration], Phys. Lett. B **583** (2004) 41 [hep-ex/0311028].
7. H1 Collaboration, contributed paper to EPS-HEP07, H1prelim-07-062, available at http://www-h1.desy.de/h1/www/publications/htmlsplit/H1prelim-07-062.long.html
8. ZEUS Collaboration, contributed paper to EPS-HEP07, ZEUS-prel-07-011, available at http://www-zeus.desy.de/~osamu/public/electron_eps2007_public.htm
9. H1 and ZEUS Collaborations, contributed paper to EPS-HEP07, H1prelim-07-166, ZEUSprelim-07-024, available at http://www-h1.desy.de/h1/www/publications/htmlsplit/H1prelim-07-166.long.html
10. A. Aktas *et al.* [H1 Collaboration], Phys. Lett. B **602** (2004) 14 [hep-ex/0408044].
11. H1 Collaboration, contributed paper to EPS-HEP07, H1prelim-07-061, available at http://www-h1.desy.de/h1/www/publications/htmlsplit/H1prelim-07-061.long.html

THE FIRST A FEW fb^{-1} : POTENTIAL FOR OBSERVING SUSY AND HIGGS

S. TSUNO
on behalf of ATLAS and CMS Collaborations
High Energy Accelerator Research Organization, KEK, Oho 1-1, Tsukuba, Ibaraki 305-0801 Japan

We outline the expected sensitivity of the discovery for SUSY and Higgs on the first few fb^{-1} operation of LHC. We also briefly introduce the global strategy for finding the SUSY particles, and proposed background estimation methods by data-driven analysis. This report contains both results from ATLAS and CMS experiments. With a few fb^{-1} data, both experiments will discover SUSY particles over wide range of the SUSY parameters, and possibly discover the SM Higgs boson in the first few year operation of LHC.

1 Introduction

The LHC is a proton-proton collider machine with a center-of-mass energy of 14 TeV at CERN in Switzerland. The CMS and ATLAS detectors are located on their collision points in the LHC ring, aiming to cover a wide range of physics programs in the hadron collider. In this letter, we will focus on the potential for the early discovery of SUSY particles and Higgs bosons. Needless to say, understanding of the detector is fundamental for the early operation of LHC running. We however introduce the baseline analysis strategy proposed in Physics Readiness Reports [1,?] rather than having a discussion about the performance of the detectors.

The key issue of the physics analysis at LHC is how we handle a significant amount of the QCD backgrounds over a signal statistics for the individual search channel. One may require so high rejection to the lepton or photon identifications against QCD jets. One may also require to be very large missing transverse energy and high-energetic multi-jets in the final state to avoid those events. As an example, the typical SUSY events ($\tilde{g}\tilde{g}$) or SM Higgs bosons (m_H=150GeV) would be possibly produced with the cross sections σ $\sim$10 pb, which corresponds to the production rate of one event every two minutes in collision at the luminosity 10^{33}cm^{2}s^{-1}. On the other hand, QCD di-jets events with $E_T \geq 100$ GeV is roughly produced with order of $\sigma \sim$1 mb, which corresponds to 1 kHz at 10^{33}cm^{2}s^{-1}. In W or Z boson production, the production rate

with $100 \sim 200$ Hz is expected. If the discovery is performed by simple counting approaches, the order of 10^{5-8} background rejection has to be achieved. This means it requires extremely high rejection performance of the backgrounds while keeping large acceptance of the signal events. In addition, the data-driven analysis methods not to rely on the Monte Carlo prediction by using the real data are desired to estimate the background contribution. Using unique event topology, one may make use of the kinematic variables. An example is the anti-tag method or masking method to evaluate the background shapes by using the similar kinematic configuration in the well-known data control sample. They are described later section.

In this paper, we start addressing the inclusive SUSY searches at first, then describe model specific SUSY searches and then followed by Higgs searches. The target luminosity for the discovery in this context is around $1 \sim 2$ fb^{-1}, so that a model independent and cut-based analysis is rather preferred with respect to the majority of importance for the understanding of the detectors.

2 SUSY searches

There are several reasons to motivate a new physics beyond the Standard Model: the electroweak symmetry breaking, hierarchy problems, gravitational force, and so forth. The Supersymmetry (SUSY) is one of the most attractive theory to resolve those issues. And this theory also inspires a good candidate of the cold dark matter. To satisfy the above condition, the supersymmetric particles tend to be degenerated at Tev-scale region. Suppose the R-parity is conserved, the model predicts new signatures that can be seen at the experiments as the unique event topology. The SUSY particles sequentially decay into another SUSY particles with lower mass eigenstates. Then, they leave at least two high mass undetected neutralinos afterwards. The typical SUSY events hence would have large missing transverse energy, multi-jets and leptons in the final state. Based upon the allowed parameter space, some benchmark points [3] have been used for the analysis.

The event topology from various SUSY cascade chains is so complicated that the "inclusive" search, based on the signature-oriented analysis, is the first approach for the discovery. Since the inclusive search does not result in such a clear resonance peak, it is often hard to distinguish new phenomena from the SM background processes. The multi-jets searches are sometimes overwhelmed by the SM processes, so that the lepton(s) may be also required in the final state even through the rates are often suppressed. Both ATLAS and CMS analyze the inclusive SUSY events categorized by the number of leptons in the final state. In addition, as the baseline selection for the inclusive searches, a very large missing transverse energy (≥ 100 GeV) and high energy multi-jet (≥ 100 GeV, at least 3-jets) events are required. Note that one remarkable difference between ATLAS and CMS SUSY inclusive searches is that ATLAS categorizes the events by the number of leptons exclusively, while CMS categorizes inclusively. Readers may refer [1,?] for details.

Figure 1 and 2 show the missing transverse energy and effective mass distributions for the typical SUSY events at 1 fb^{-1}. One can find a huge event excess ($\sim$5000 events) of the SUSY events. Against of the rapid decrease of the SM backgrounds, the SUSY events tend to result in the large contribution in the tail region over a wide range of parameter space. Thus, understanding of the tail structure of those distributions for the SM backgrounds is the most important task. Since the large missing p_T distribution caused by the SM processes most likely comes from the mis-measurement of the missing p_T such that a jet goes in the crack region of detector and they are weakness part of the theoretical prediction, the data-driven background estimation methods are strongly desired.

The proposed background estimation methods by the data in ATLAS and CMS are as follows. The dominant background is $Z \rightarrow \nu\nu$+jets, W+jets and $t\bar{t}$+jets. The $Z \rightarrow \nu\nu$+jets

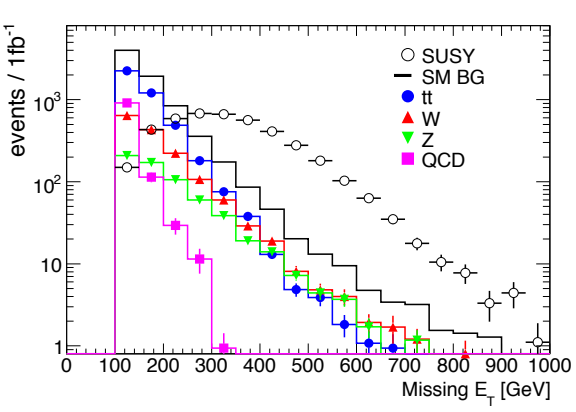

Figure 1: Missing transverse energy for the typical SUSY events at 1 fb^{-1} (ATLAS).

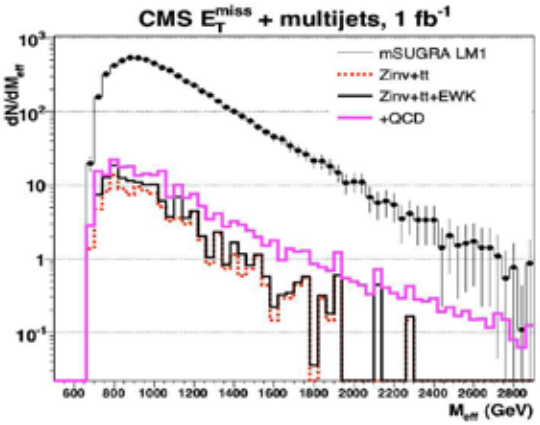

Figure 2: Effective mass distributions for the typical SUSY events at 1 fb^{-1} (CMS).

events are estimated by using $Z \to \mu\mu$+jets events. The identified di-muon events are replaced to two neutrinos, then the missing transverse energy is re-calculated. Since the production mechanics are same in both processes, after the correction of the muon reconstruction efficiency and scaling to the neutrino branching ratio, the missing transverse energy is correctly estimated by the $Z \to \mu\mu$ events in data. Figure 3 justifies to reproduce the original missing p_T distribution of $Z \to \nu\nu$ process by the $Z \to \mu\mu$ events after masking their muons. The normalization is simply given by the relative-ratio of the branching ratio of $Z \to \nu\nu$ to $Z \to \mu\mu$. For the $t\bar{t}$ and W+jets backgrounds, the transverse mass distribution is used in the lepton+MET+jets events because the transverse mass has no correlation to the final effective mass distribution. In low transverse mass region, as shown in Figure 4, the $t\bar{t}$ and W + jets events are dominated. The fraction of W + jets events to $t\bar{t}$ events does not depend on the cut of the transverse mass distribution, so that this fraction is valid in the signal region. Thus, we can use low transverse mass region as the control sample. The shape is drawn by the control sample, then overall normalization is taken into account the low missing p_T region in which the SUSY signal does not contribute. Finally, the QCD multi-jet events is estimated by using the various kinematical configurations or the anti-tag methods in the object identification. As mentioned, in most of case, the large missing p_T by the QCD multi-jets events is from the mis-measurement of the energy in calorimeters. In such a case, the direction of the missing p_T has strong correlation to the observed jets, where the direction of the fake missing p_T is most likely back-to-back with respect to the leading jet. Thus, one of major estimation method is to use the ϕ-correlation between jets and missing p_T. Using the phase space where QCD jet events are enhanced as control sample, the QCD shape and normalization are driven by the data control sample. One should also note that the semi-leptonically decayed b-jets are also major source of the large missing p_T background. The situation is even more complicated, where the dedicated studies are necessary.

In the di-lepton mode, the end-point of the di-lepton invariant mass distribution is used to determine the mass difference of the SUSY particles. For instance, if a squark $\tilde{q}$ has the decay chain of $\tilde{q}_L \to \tilde{\chi}_2^0 q \to \tilde{\chi}_1^0 l^{\pm} l^{\mp} q$ and $\tilde{\chi}_0^1$ is LSP, the di-lepton invariant mass edge contains an information of the mass difference of $\tilde{\chi}_0^2$ to $\tilde{\chi}_0^1$ by simple kinematical requirement. Then, the end-point is measured by the flavor subtraction method. In the SM processes, the leptons from weak boson decay have the same branching ratio not depend on the lepton flavor. Thus, since most of leptons come from the weak boson decay when high p_T leptons are required, the SM processes are canceled out by using the relation of $N_{ee} + \beta^2 N_{\mu\mu} - \beta N_{e\mu}$, where β is the efficiency correction of muon to electron. We demonstrate this feature in Figure 5. The $t\bar{t}$ background are

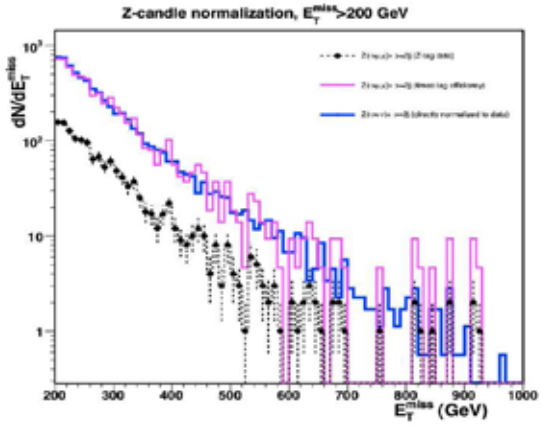

Figure 3: Missing transverse energy for the two processes rescaled $Z \to \mu\mu$ and true $Z \to \nu\nu$ (CMS). Different histogram (black-solid-marker) expresses before rescaling of the $Z \to \mu\mu$ events.

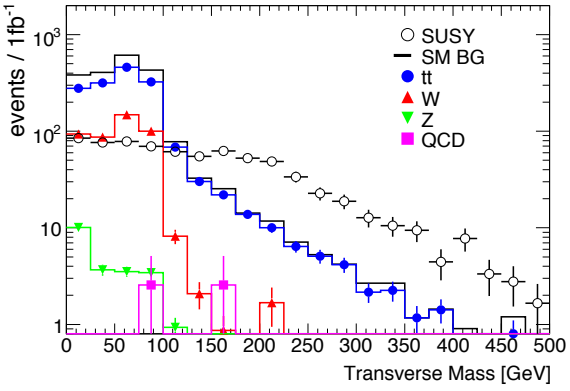

Figure 4: Transverse mass distribution of signal and background events (ATLAS). Low transverse mass region (M_T ≤100GeV) is used as the control sample.

only shown in the plot, but the SM contribution fairly cancels and then the large event excess by SUSY events is left. The signal event statistics is enough to determine the end-point of the mass distribution. This technique is very powerful not only for the background suppression like a requirement of the same signed di-lepton events but also for the direct measurement of the SUSY particles.

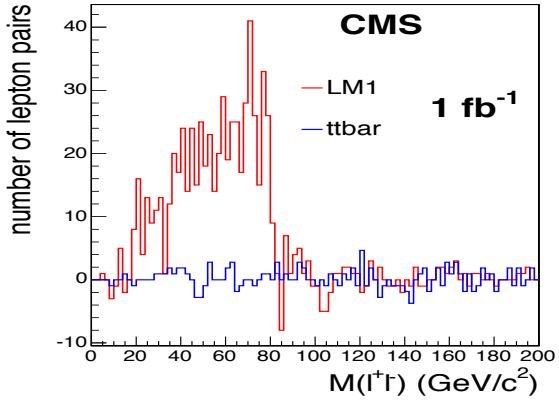

Figure 5: Di-lepton invariant mass distribution after flavor subtraction (CMS). The $t\bar{t}$ background are only shown in the plot.

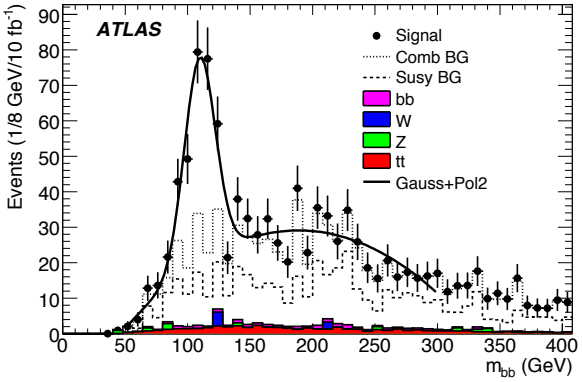

Figure 6: Invariant mass distribution by $H \to b\bar{b}$ in the SUSY events (ATLAS).

In the particular parameter space, the SUSY particles also allow to decay into Higgs or Z bosons. In this case, the search is to look for the mass resonance in addition to the large missing p_T requirement. Requiring the di-lepton pair for the resonance peak, high mass resolution is obtained. As the other example, Figure 6 shows the mass distribution by $H \to b\bar{b}$ in the SUSY events. The large missing p_T cut is already imposed, so that the SM background events do not contribute. This mode has extremely high potential to discover the SUSY events in this particular parameter space.

We present the expected discovery potential from ATLAS and CMS in Figure 7, where note that CMS shows only muon channel. With 1 fb^{-1} data, both experiments covers a wide range of SUSY parameter space for the discovery.

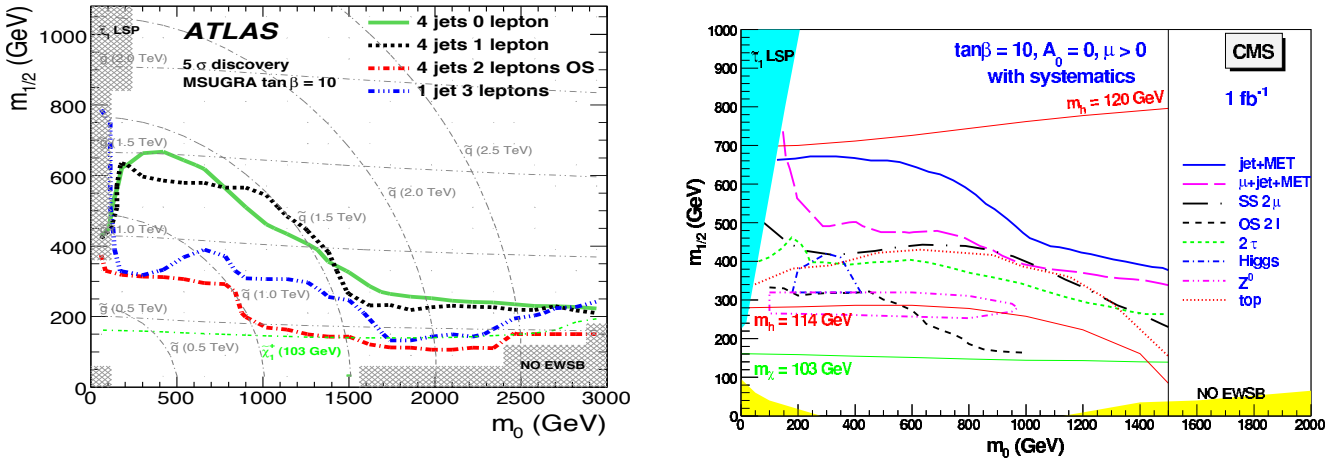

(a) (b)

Figure 7: 5σ SUSY discovery potential from (a) ATLAS and (b) CMS at 1fb^{-1}, respectively. The CMS results only show the muon channel.

3 Higgs searches

Despite the remarkable success of the Standard Model in high energy physics during the recent decades, nothing is known about the source of its fundamental theoretical basis, the Higgs mechanism. The search for the Higgs bosons has been considered to be the most important subject in LHC. In 14-TeV proton-proton collision at LHC, the SM Higgs boson is predominantly produced via gluon-fusion production process. The search channels thus depend on the Higgs mass and its decay mode. Since the recent top-quark and W-boson mass measurements [4] at Tevatron Run II suggest to have a low-mass Higgs boson, the low-mass SM Higgs search is the primary topics for early discovery. The promising decay mode are $H \to \gamma\gamma$, $H \to ZZ \to 4l$ and $H \to WW \to ll\nu\nu$ modes for the early discovery. The mass resolutions are about 1~2 GeV for the $H \to \gamma\gamma$ and $4l$ channels while the $ll\nu\nu$ channel has the largest production cross section although the invariant mass is not reconstructed. The achievement of a good performance of the lepton and photon identifications and energy resolution are essential for those analyses. We show an example of the reconstructed invariant mass for $4l$ channel in Figure 8. The number of events corresponds to 10 fb^{-1} luminosity. We can see the large resonance peak in $4l$ channel. In $ll\nu\nu$ channel, the transverse mass is reconstructed and predicts the large excess of the signal events.

In addition to the gluon-fusion process, the second largest production mechanics is the Vector-Boson fusion process (VBF) [5]. In the VBF process, the incoming quarks are scattered off the heavy vector bosons to form the jets in the forward and backward region. This provides additional means to suppress the backgrounds[6]. The correlation between two forward jets is used to separate the signal events from the background events. The separation in the pseudorapidity $\Delta\eta$ for two jets strongly suppresses the background events. Also, according to the presence of high energetic two forward jets, the di-jet mass can reject the background events. Furthermore, since the signal event does not much produce jets in central region due to a nature of the color-connection in VBF production process, the central jet veto may be imposed. In Figure 9, the di-photon invariant mass distribution for $H \to \gamma\gamma$+2jets channel is shown at 30 fb^{-1} data. This is a new result in ATLAS. The analysis with two photon events is categorized by the number of jets. The backgrounds are largely suppressed by the forward jets requirement.

While the VBF selection is applied to reject the backgrounds, the minimal supersymmetric

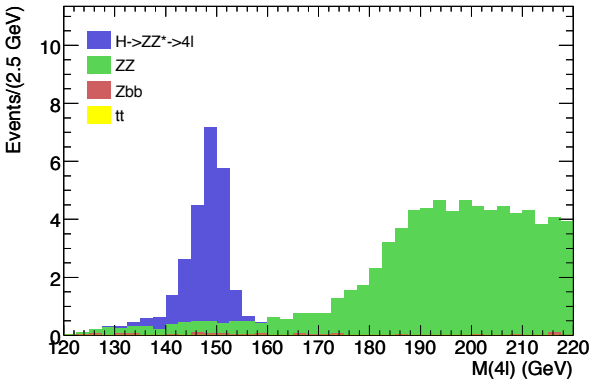

Figure 8: Reconstructed invariant mass with m_H=150 GeV for $4l$ channel at 10 fb^{-1} data (ATLAS).

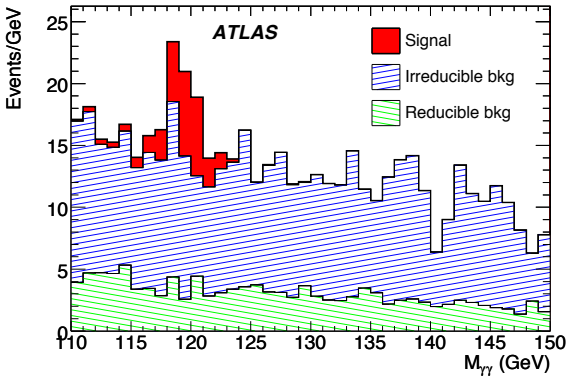

Figure 9: Di-photon invariant mass distribution for $H \to \gamma\gamma$+2jets channel at 30 fb^{-1} data (ATLAS).

extension of the Standard Model (MSSM) predicts larger production cross sections for the Higgs bosons over a wide parameter range since they have large couplings with down-type fermions in large $\tan\beta$ region. The production associated with a bottom quark is a promising search channel in this case. The $H \to \tau\tau$ and $H \to \mu\mu$ channels are analyzed. Also, the b-jet tagging are valid tool to enhance the signal events over QCD backgrounds. The branching ratio of Higgs decaying to τ is much larger than that to μ. On the other hand, the mass reconstruction by the muon pair has much better resolution than that by the τ-pair. The sensitivity of this analysis is a trade-off of the signal statistics or high mass resolution.

Finally, we present the SM Higgs discovery potential expected in ATLAS and CMS experiments at 30fb^{-1} data in Figure 10 (a) and (b), respectively. Note that at that time being in ATLAS, the $H \to \gamma\gamma$+ 2jets analysis was not included in this sensitivity. Both experiments fully cover in almost full mass-range. Even within 1∼5 fb^{-1} data, it can reach at 5σ discovery for the high mass region.

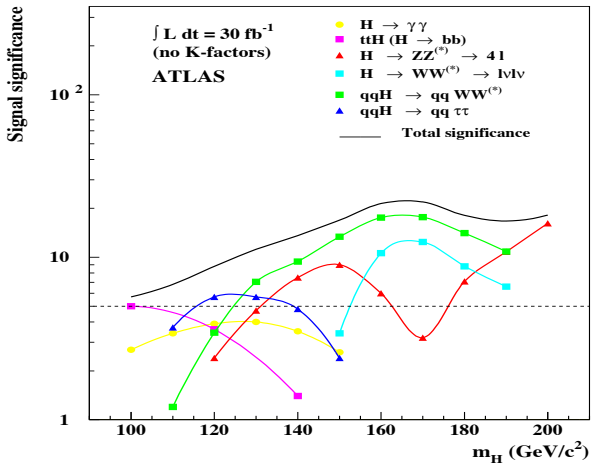

(a)

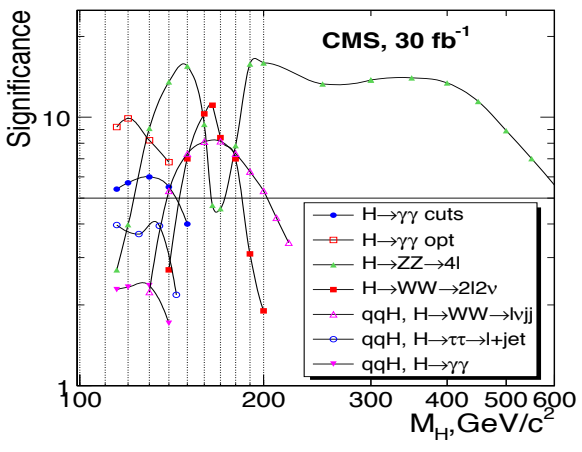

(b)

Figure 10: The SM Higgs discovery potential expected in ATLAS and CMS experiments at 30fb^{-1} data.

4 Summary

The LHC is so-call the discovery machine. With 14-TeV proton-proton collision and high design luminosity, the ATLAS and CMS experiments will discover a new physics and/or Higgs bosons even with a few fb^{-1} data.

For SUSY searches, the inclusive search is the most promising search channel in that the observed signature does not depend on the SUSY models. Many of the parameter space in mSUGRA is expected to be covered for their discovery reach. In the analysis, the understanding of the tail structure of the missing transverse energy is very important to estimate the background contribution. The data-driven background estimation methods are desired. Fortunately, the LHC has an unique opportunity that even abundant SM physics processes theirselves become a kind of calibration processes to evaluate the event topology, where the event statistics is not matter in the SM processes. Using similar event topology, one may obtain a shape of the backgrounds and the associated shape uncertainty. In the di-lepton edge analysis, it indicates the mass difference of the SUSY particles, and reveals the nature of the SUSY model. If SUSY particles exist, this is the most powerful method to determine the model. The search for the resonance peak does not also require the specific model. It will be useful to determine or constrain the parameter space of the model.

In Higgs searches, the $H \to ZZ \to 4l$ and $WW \to l\nu l\nu$ channels are the most promising discovery channels in the early data in LHC. In addition to the analysis based on the gluon fusion production process, the analysis with the VBF production processes further increases the signal sensitivity to the backgrounds. In low mass region, the $H \to \gamma\gamma$ channel has the largest sensitivity. Both inclusive and VBF analyses are performed. With $1\sim5$ fb^{-1} data, the SM Higgs boson will be discovered for a wide range of mass-spectrum. Note that within the framework in the MSSM, the MSSM Higgs sensitivity is further increased, according to the strength of the couplings with fermions.

The first collision is expected to be made with 10 TeV on the summer 2008. Then, the 14-TeV physics run will turn on after a short running of 10-TeV commissioning, so that the first physics results will be successively followed by the next year. The Physics Readiness Report from both experiments has been prepared. In ATLAS, the latest report will be available soon, where all physics analysis respect the analysis computing model in the real data analysis. The MC data are distributed and analyzed on the grid as the part of the computing system commissioning (CSC). Most of results presented in the last TDR will be replaced to the CSC results. In this paper, a few selected CSC results are presented. There are many attractive updated results as well as completely brand-new results in the CSC report. And this report will be the final before real-data come out. We, LHC experimentalist, are waiting for the real-data with the most sophisticated prediction with our best knowledge.

Acknowledgments

The author would like to thank all the people in the ATLAS and CMS Collaborations, and especially physics conveners from both experiments for helping useful comments. The author would also like to thank the organizers of the Conference.

References

1. CMS Physics TDR, CERN-LHCC-2006-001 (2006).
2. ATLAS Physics TDR, CERN-LHCC-99-15 (1999).
3. A.De. Roeck, *et al*, *Eur. Phys. J.* C **49**, 1041 (2007).

4. The LEP Electroweak Working Group, http://lepewwg.web.cern.ch/LEPEWWG/ , Tevatron New Phenomena and Higgs Working Group, arXiv:hep-ex/0804.3423v1.
5. D.L. Rainwater, *et al*, *Phys. Rev.* D **59**, 014037 (1999).
6. S. Asai, *et al*, *Eur. Phys. J.* C **32S2**, 19 (2004).

THE FIRST FEW FB^{-}1; POTENTIAL FOR OBSERVATION OF PHYSICS BEYOND THE STANDARD MODEL

R. BELLAN, on behalf of ATLAS and CMS Collaborations
European Organisation for Nuclear Research (CERN), Geneva, Switzerland

An important part of the ATLAS and CMS program is to search for new physics beyond the Standard Model. Some of the main ongoing studies are presented by signature, with particular emphasis on those channels already observable with the first collected data. Here only non-super-symmetric models are presented, as susy models are discussed elsewhere [1].

1 Introduction

LHC will offer the possibility to observe or set limits on new physics beyond the Standard Model (SM), using relatively few data. Many models can suddenly be investigated, although early data may not be enough to identify the model that describes the signal.

In the following sections the signatures of some of the main searches at LHC are discussed.

2 Jet Final States

Inclusive di-jet production ($pp \rightarrow 2$ jets + anything) is the dominant LHC process. To lowest order it arises from the $2 \rightarrow 2$ QCD scattering of partons in which only coloured particles are involved in the initial, intermediate and final states.

Di-jet resonances and contact interactions are the two major signals of new physics with di-jets [2]. Di-jet resonances produce compelling signals of a new particle at a mass M, but require that the incoming parton-parton collision energy to be close to that mass (which must be kinematically accessible). Contact interactions produce more ambiguous signals but come from an energy scale of new physics, Λ, which can be significantly larger than the available collision energy, thus allowing to probe a wider energy spectra. In both cases the observables

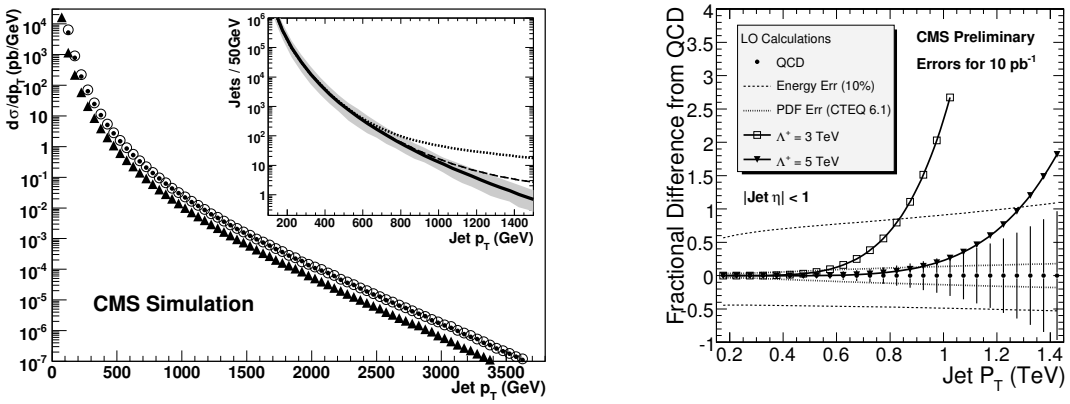

Figure 1: (Left) Inclusive jet differential cross section expected from QCD for $|\eta| < 1$ as a function of jet p_T for generated jets (points), jets (triangles), and corrected jets (open circles). The inset shows the number of generated jets for an integrated luminosity of 10 pb^{-1}. The size of a 10% uncertainty in the jet energy scale (shaded band) is shown centred on the QCD background (solid). The signal from a contact interaction is shown for scale $\Lambda^+ = 3$ TeV (dotted) and $\Lambda^+ = 5$ TeV (dashed). (Right) Fractional difference with respect to QCD as a function of jet momentum. This variable unambiguously shows the discrepancy between the expected QCD background and the signal (Λ^+) for jet-p_T above 1 TeV.

used to study such processes are very simple. In the inclusive jets analysis the number of jets inside an η window are counted as a function of the jet p_T. For the di-jets study, the two jets with highest p_T, and inside a given pseudorapidity region, are selected and counted as a function of the invariant mass of the di-jet system.

2.1 Sensitivity to Contact Interactions: Inclusive Jet-p_T Study

New physics at a scale above the energy scale of the process can be effectively modelled as a contact interaction. The canonical contact interaction studied in hadron collisions arises from the following left-left isoscalar colour-singlet term which is added to the QCD Lagrangian [3]:

$$L_{qq} = \frac{Ag^2}{2\Lambda^2}(\bar{q}_L\gamma^\mu q_L)(\bar{q}_L\gamma_\mu q_L) \quad (1)$$

where $A = \pm 1$ determines the sign of the interference with QCD, Λ is the contact interaction scale and the square of the coupling g^2 is by convention set equal to $4\pi\alpha_s$. $\Lambda^\pm$ is a compact notation commonly used to include the choice $A = \pm 1$.

Contact interactions produce a rise in rate, relative to QCD, at high inclusive jet p_T as shown in Figure 1. The figure shows the jet rates, expected for an integrated luminosity of 10 pb^{-1}, using a simulation of the CMS experiment. A contact interaction with a scale of $\Lambda^+ = 3$ TeV clearly produces a large rate compared to QCD expectation for jet $p_T > 1$ TeV, event taking into account a 10% energy scale uncertainty.

2.2 Sensitivity to di-Jets Resonances: Di-Jet Mass Spectrum Study

Many models predict narrow di-jet resonances [4]. In Figure 2 the cross section for an excited quark di-jet resonance to the statistical uncertainties expected on the QCD di-jet background are compared for a luminosity scenario of 10 pb^{-1}. The normalisation of the excited quark signal come from the lowest order calculation. Figure 2 illustrates that the di-jets channel is sensitive to an excited quark signal up to several TeV. With only 10 pb^{-1} a 2 TeV excited quark signal begins to emerge above the statistical error bars with a total significance of 4.1, neglecting systematic uncertainties.

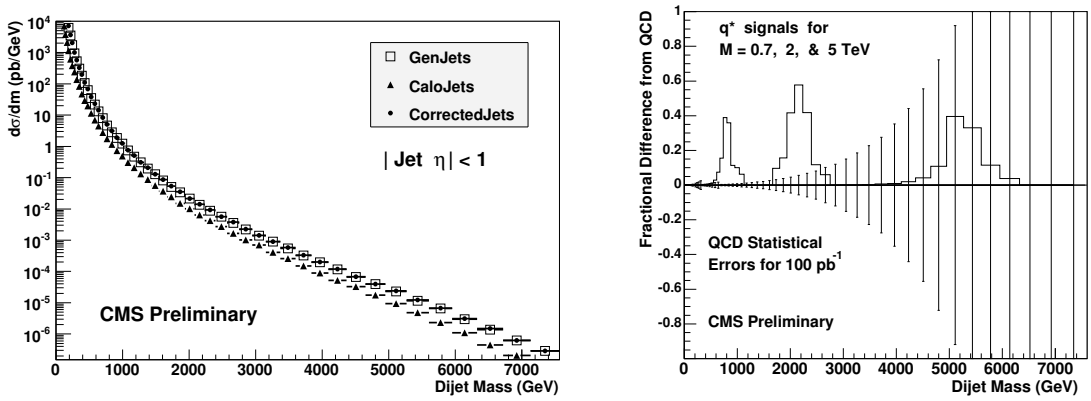

Figure 2: (Left) Di-jets differential cross section expected from QCD for $|\eta| < 1$ as a function of the di-jets invariant mass, for generated jets (points), jets (triangles), and corrected jets (open boxes). (Right) Fractional difference with respect to QCD as a function of di-jets invariant mass, in case of excited quark signal.

3 High Invariant Mass of di-Lepton Final States

In a hadron collider the final states with leptons are a clear signature for many processes, in particular di-lepton final states are naturally the best candidate for discovery of new physics beyond Standard Model. Many models predict either resonances or deviation from the SM differential cross section ($d\sigma/dm_{ll}$) of the process [4].

The main characteristics of the signal are the high momenta of the leptons, which are also isolated, and the large invariant mass of the lepton pair. The most important background is the Drell-Yan process, although its cross section is vanishing at the energy scale at which new physics is expected. The same signature is shared by many models and this would make difficult the identification of the correct theory using only early data. From the experimental point of view, due to the characteristics of the particles in the final state, the detection, reconstruction and identification of such leptons can be at the limits of the performance of the apparatus, depending on the energy scale at which the new process arises. Therefore a high-level understanding of the alignment [5] and calibration [6] of the detector is fundamental for the discovery.

3.1 Resonances in Final States: New Neutral Gauge Bosons

Additional heavy neutral gauge bosons (Z') are predicted in many superstring-inspired [7,8] and grand unified theories [9], as well as in dynamical symmetry breaking [10] and little Higgs [11] models. However, there are no reliable theoretical predictions of the Z' mass scale. Current lower limits on the Z' mass are (depending on the model) of the order of $600 - 900$ GeV/c^2 [12].

The Z' most frequently discussed and whose properties are representative of a broad class of extra gauge bosons are:

- Z_{SSM} within the Sequential Standard Model (SSM), which has the same couplings as the Standard Model Z^0.
- Z_ψ, Z_η and Z_χ, arising in E_6 and $SO(10)$ GUT groups.
- Z_{LRM} and Z_{ALRM}, arising in the framework of the so-called left-right and alternative left-right models.

The LHC offers the opportunity to search for Z' bosons in a mass range significantly larger than 1 TeV/c^2, already with the first data [5]. In Figure 3 the summary plot shows that already with 100 pb^{-1} a region not yet explored by Tevatron experiments can be studied.

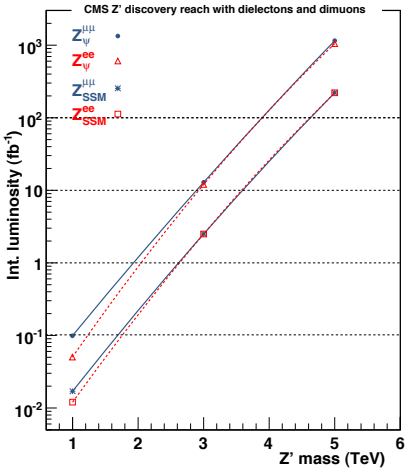

Figure 3: Z' discovery reach for two of the models studied in the di-lepton channels at CMS experiment. The reach of the rest of the models studied is within the band defined by Z_SSM and Z_ψ.

The Z' is not the only neutral vector boson that can be seen in leptonic channels. Randal-Sundrum (RS) models [13] predicts massive Kaluza-Klain (KK) modes of the graviton (G_{RS}).

Most collider physics phenomenology done with warped extra dimensions so far is based upon one very specific model, the original simple scenario called RS1. In RS1, the Standard Model is replaced at TeV scale by a new effective theory in which gravity is still very weak, but there are exotic heavy spin-2 particles.

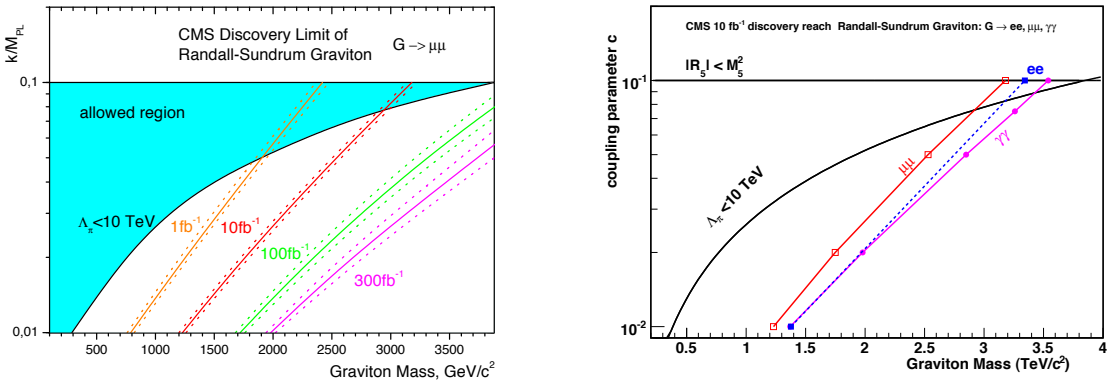

Figure 4: RS graviton discovery mass reach (at CMS) as a function of the model coupling parameter in the di-muon muon channel (left). The curves include the systematics uncertainty. On the right the comparison between the sensitivity of the different channels, shown for an integrated luminosity of 10 fb^{-1}.

At LHC the KK gravitons of RS1 would be seen as di-fermion or di-boson resonances. In particular, with early data, only the first excitation of the RS graviton can be accessible.

In Figure 4-(left) the reach of the CMS experiment [5], for RS1 graviton in muon channel, is shown as a function of the coupling parameter (k/M_{PL}, where k is the curvature of the warped extra dimension and M_{PL} is the Planck mass in 5 dimensions) and the graviton mass. The ranges of the expected variations due to the systematic uncertainties are also drown: 1 fb^{-1} is enough to explore a wide part of the region allowed by the theory.

Early data could not be enough to perform detailed angular distribution studies (crucial in order to distinguish a spin-1 particle, like the Z', with respect to a spin-2 one, like the G_{RS}), however some handle is given by looking at resonances in some final states, which are precluded

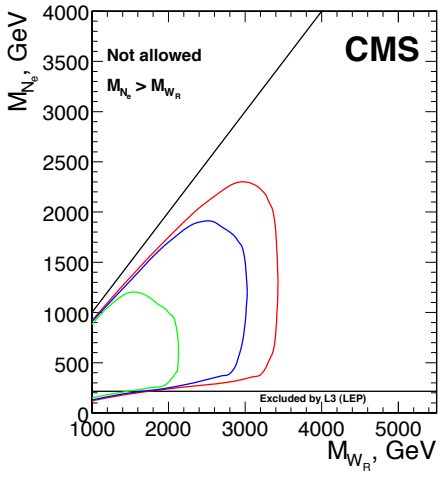

Figure 5: CMS discovery potential of the W_R boson and right-handed Majorana neutrinos of the Left-Right Symmetric model for an integrated luminosity of 1, 10 and 30 fb^{-1}.

in the other models due to the nature of the new particle. In fact, while the the Z' cannot decay into a pair of vector bosons, the RS graviton can. In Figure 4-(right) the sensitivity of the analysis to the $G_{RS} \to \gamma\gamma$ channel is also drown and shown to be comparable with the leptonic final states, thus allowing a cross-check of the resonance, even with a few collected data. The G_{RS} branching ratio to photons is roughly twice that of electrons or muons, however the reach for low coupling and graviton mass is comparable between di-leptons and di-photons due to the QCD and prompt photon backgrounds in the photon channel which are harder to efficiently suppress. For higher masses and coupling the di-photon is leading the reach due to the higher branching ratio. The di-muon channel is trailing the reach compared to the di-electrons merely due to resolution.

4 Two Leptons and Two Jets Final State

4.1 Heavy Majorana Neutrinos and right-handed bosons

The two leptons and two jets final states can be a clear signature of process described by left-right symmetric model $SU_c(3) \otimes SU_L(2) \otimes SU_R(2) \otimes U(1)$ [14,15]. The model embeds the SM at the scale of the order of 1 TeV and naturally explains the parity violation in weak interactions as a result of the spontaneously broken parity. It necessarily incorporates three additional gauge bosons W_R and Z' and the heavy right-handed Majorana neutrino states N. The N particles (N_l) can be the partners of the light neutrino states ν_l ($l = e,\ \mu,\ \tau$) and can provide their non-zero masses through the seesaw mechanism [16].

The direct searches for W' at the Tevatron yield bounds $M_{W'} \gtrsim 720$ GeV/c^2 assuming a light (keV-range) N, and $M_{W'} \gtrsim 650$ GeV/c^2 assuming $M_N \gtrsim M_{W'}/2$ [17]. These bounds are less stringent in more general LR models.

The cross section of $pp \to W_R \to l + N_l + X$, where $N_l \to l + j_1 + j_2$, depends on the value of the coupling constant g_R, the parameters of the CKM mixing matrix for the right-handed sector, the W_R-W_L and Z'-Z mixing strengths, and the masses of the partners N_l of the light neutrino state. In the study presented here the mixing angles are assumed small, the right-handed CKM matrix identical to the left-handed one and $g_R = g_L$. Finally it is assumed that only the lightest M_{N_e} is reachable at LHC. In the case of degenerated masses of N_l, the channels with μ's and τ's are open resulting in the increase of the cross section of the process studied here by a factor of 1.2. The two major backgrounds considered in this study are the inclusive production of Z

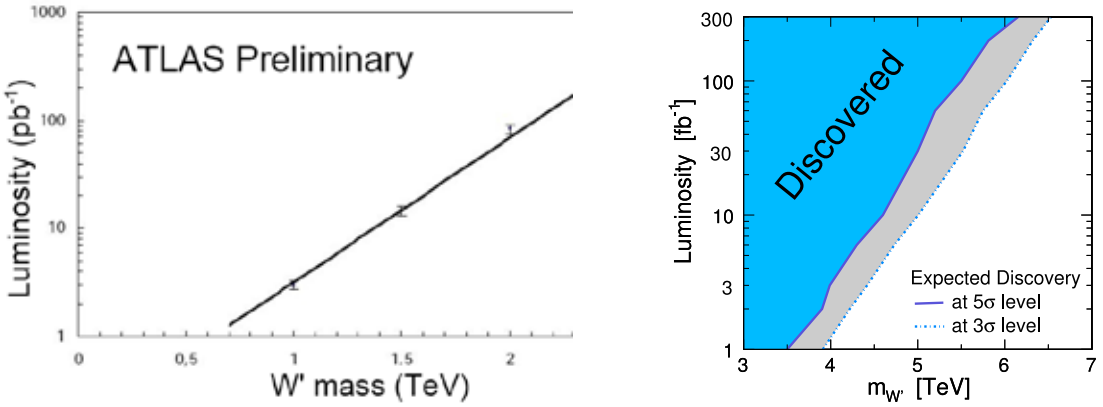

Figure 6: Integrated luminosity needed to discover (at 5 sigma level) a W' boson, depending on its mass, at ATLAS (left) and CMS (right).

and $t\bar{t}$. In the event selection two isolated electrons and at least two jets are required.

The 5 sigma discovery contour in the (M_{W_R}; M_{N_e}) plane is shown in Figure 5 for an integrated luminosity of 1, 10 and 30 fb^{-1} (CMS experiment simulation [5]). With 1 fb^{-1} a 5 sigma observation of W_R and N_e, with masses up to 2 TeV/c^2 and 1 TeV/c^2 respectively can be achieved.

5 Leptons and Missing Energy Final States

As mentioned in Section 3.1 many models predict additional heavy gauge boson, including charged particle. Here are presented the detection capabilities for a hypothetical heavy partner of the Standard Model W, a charged spin-1 boson W', with the properties from the Reference Model by Altarelli [18]. In this model, the W' is a much massive copy of the W, with the very same left-handed fermionic couplings (including CKM matrix elements), while there is no interaction with the Standard Model gauge bosons or with other heavy gauge bosons as a Z'. Thus the W' decay modes and corresponding branching fractions are similar to those for the W. In hadron collisions W' bosons can be created through $q\bar{q}$ annihilation, in analogy to W production. Previous searches for the reference W' at LEP and at the Tevatron give rise to lower bounds approaching 1 TeV [12].

Given that the W' boson has a large mass, it is likely to be produced without transverse momentum. Due to a boost along the z-axis, the angle between the muon and the neutrino might be different from π in the laboratory system. However, the angle in the transverse plane stays invariant under boosts along the z-axis. Therefore the signature of a W' event is high energy isolated muon, together with a large amount of missing energy pointing to the opposite direction in the transverse detector plane. Due to the small transverse momentum of the W' boson, the transverse momentum of the muon and the missing transverse energy are of similar magnitude.

In Figure 6 the discovery potential of both ATLAS [19] and CMS [5] is shown. Less than 1 fb^{-1} is needed to find a signal with a significance at 5-sigma level.

6 Black Hole

One of the consequence of large extra dimension is the possibility to produce microscopic black hole at LHC energy[20,21]. From a semi-classical calculation the cross section of the black hole

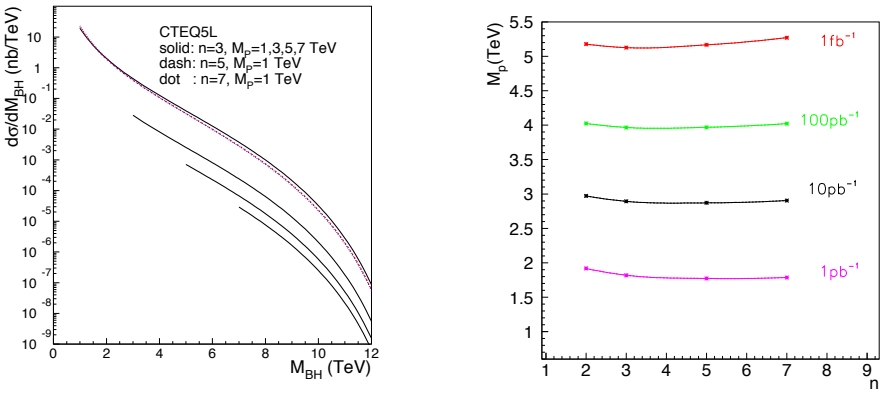

Figure 7: (Left) Differential cross section of the black hole production, as a function of a black hole mass for each (M_{PL}, n) parameter. (Right) Contours of the integrated luminosity needed for a 5 sigma discovery, plotted in the (M_{PL}, n) plane.

production can be written as

$$\sigma(M_{BH}) = \pi r^2_{s(4+n)}$$

where $r^2_{s(4+n)}$ is the Schwarzschild radius in "4+n" dimensions.

Considering a black hole mass much larger than the Planck mass in 4+n dimensions (M_{PL}), and assuming the latter to be of the order of the TeV scale, then $\sigma(M_{BH}) \sim$ pb [a].

The black holes have a very short life time, predicted to be of the order of 10^{-12} fs and are expected to evaporate democratically by emission of all particle types that exist in nature, independent of their quantum numbers or interaction properties. Therefore they can be a source of new particles. Black holes would also be able to provide the possibility of probing quantum gravity.

Requiring M_{BH} to be larger than M_{PL}, potentially the black hole observation can be accomplished within an integrated luminosity of 1 fb^{-1} in all cases of n and if M_{PL} is less than 5 TeV, as shown in Figures 7.

7 Summary

The Large Hadron Collider will give the possibility to shade light on new physics and models. Here some examples of the phenomena that could be discovered with few data collected at ATLAS and CMS have been reviewed. In Table 1 a summary of such discoveries are reported. Although the understanding of the detector will be crucial for a claim of an observation of a new signal, both experiment show a high discovery potential already with an integrated luminosity of few fb^{-1}.

[a] Recent studies claims that due to the "Apparent Horizon" effect, the event horizon is not formed as fast as needed, thus a large fraction of the initial energy could escape before the black hole is formed. This implies that more partonic energy is needed to form the black hole than the one predicted by the naive semi-classical calculation. In such a scenario the black hole cross section is a few orders of magnitude smaller than the above calculation.

Table 1: Summary of the principal discoveries accessible with the first data taken at LHC.

Model	Mass Reach (TeV)	L (pb^{-1})	Early Systematic
Contact interaction	$\Lambda \sim 2.8$	10	Jet efficiency and energy scale
	Z'		
ALRM	M$\sim$1	10	
SSM	M$\sim$1	20	Alignment
LRM	M$\sim$1	30	
E_6, SO(10)	M$\sim$1	30-100	
Technirho	M$\sim$[0.3]	100	Jet energy scale
Axigluon or Colouron	M$\sim$[0.7,3.5]	100	Jet energy scale
Excited quark	M$\sim$[0.7,3.6]	100	Jet energy scale
E_6 di-quarks	M$\sim$[0.7,4]	100	Jet energy scale
mUED	M$\sim 0.3 - 0.6$	10-1000	MET, jet/photon energy scale
ADD real G_{KK}	$M_D \sim 1.5$ (n=3), ~ 1 (n=6)	100	MET, jet/photon energy scale
ADD virtual G_{KK}	$M_D \sim 4.3$ (n=3),~ 3 (n=6)	100	Alignment
	$M_D \sim 5$ (n=3),~ 4 (n=6)	1000	
	RS1		
di-jets	$M_G \sim$[0.7,0.8], c=0.1	100	Jet energy scale, alignment
di-muons	M$\sim$[0.8,2.3], c=[0.01,0.1]	1000	

References

1. S. Tsuno, this proceedings.
2. The CMS Collaboration, CMS PAS SBM 07 001 (2007).
3. N. Krasnikov and V. Matveev, *Phys. Usp.* **47**, 643 (2004).
4. K. Gumus *et al.*, CMS Note 2006/070 (2006), and references therein.
5. The CMS Collaboration, CERN/LHCC 2006-021, CMS TDR 8.2 (2006).
6. B. Clerbaux *et al.*, CMS Note 2006/004 (2006).
7. M. Cvetic and P. Langacker *Phys. Rev.* D **54**, 3570 (1996).
8. M. Cvetic and P. Langacker *Mod. Phys. Lett.* A **11**, 1247 (1996).
9. A. Leike *Phys. Rept.* **317**, 143 (1999).
10. C.T. Hill and E.H. Simmons, *Phys. Rept.* **381**, 235 (2003).
11. T. Han *et al.*, *Phys. Rev.* D **67**, 095004 (2003).
12. W.M. Yao *et al.*, JPG **33**, 1 (2006) and 2007 partial update for 2008.
13. L. Randall, this proceedings.
14. R. Mohapatra and J. Pati, *Phys. Rev.* D **11**, 566 (1975).
15. G. Senjanovic and R. Mohapatra, *Phys. Rev.* D **12**, 1502 (1975).
16. R. Mohapatra and G. Senjanovic, *Phys. Rev. Lett.* **44**, 912 (1980).
17. D0 Collaboration, S. Abachi *et al.*, *Phys. Rev. Lett.* **76**, 3271 (1996).
18. G. Altarelli *et al.* , ZPC **45**, 109 (1989).
19. The ATLAS Collaboration, CERN/LHCC 99-015, ATLAS TDR 15 (1999).
20. S. Dimopoulous and G. Landsberg, *Phys. Rev. Lett.* **87**, 161602 (2001).
21. B. Giddings and S. Thomas, *Phys. Rev.* D **65**, 056010 (2002).

SEARCHES IN LEPTON FINAL STATES

SOURABH DUBE (for the CDF and DØ collaborations)
Department of Astronomy and Physics, Rutgers University.
136 Frelinghuysen Road, Piscataway, New Jersey, USA 08854

Abstract

Searches for new physics in lepton final states at the Tevatron are summarized in this paper. I describe the searches for supersymmetric particles such as chargino/neutralino and tau-sneutrino. I also describe searches for excited gauge bosons (W', Z') and excited electrons.

1 Introduction

The standard model(SM) of physics gives a successful description of natural phenomena. It is applicable over a wide range of energy scales. However, the standard model has a few unanswered questions. It does not include gravity, or describe the origins of masses of the fundamental particles. It suffers from the hierarchy problem, and gives no hints about the nature of dark matter or dark energy which constitute 96% or our universe.

There are several proposed models of new physics beyond the standard model. Supersymmetry(SUSY) is a new proposed symmetry between fermions and bosons. It posits the existence of boson superpartners to all SM fermions and vice versa. It solves the hierarchy problem and in certain models suggests an attractive dark matter candidate particle. Other models such as left-right-symmetric models (broken $SU(2)_L \times SU(2)_R$) or Grand Unification Theories which unify the electroweak and strong forces predict additional gauge bosons. The Randall-Sundrum model of warped extra dimensions predicts the existence of a massive spin-2 particle.

The search for new physics in lepton final states has many advantages over other channels. Lepton final states are relatively clean and free from backgrounds. Since identifying leptons is well understood at the CDF and DØ detectors, the backgrounds in lepton final states from SM processes are straightforward to estimate. Many new models predict leptonic final states and thus these analyses are sensitive to a wide variety of models beyond the standard model.

Results shown here use from 1 to 2.5 fb^{-1} of data from the Tevatron for each CDF and DØ

Table 1: CDF results of a search for $\tilde{\chi}_1^{\pm}\tilde{\chi}_2^0 \to lll+\not\!\!E_T$. The signal quoted is for mSUGRA model with parameters $m_0 = 60$ GeV/c^2, $m_{1/2} = 190$ GeV/c^2, tan(β)=3, $A_0 = 0$, $\mu > 0$.

Channel	Expected Signal	Background	Observed
3 tight leptons	2.3±0.3	0.5±0.1	1
2 tight + 1 loose	1.6±0.2	0.3±0.04	0
1 tight + 2 loose	0.7±0.1	0.1±0.03	0
2 tight + track	4.4±0.6	3.2±0.7	4
1 tight + 1 loose + 1 track	2.4±0.3	2.3±0.6	2

Table 2: DØ results of a search for $\tilde{\chi}_1^{\pm}\tilde{\chi}_2^0 \to lll+\not\!\!E_T$. The signal quoted is for mSUGRA-inspired model with parameters $m_0 = 88 - 121$ GeV/c^2, $m_{1/2} = 182 - 221$ GeV/c^2, tan(β)=3, $A_0 = 0$, $\mu > 0$. The RunIIb analysis is a new analysis.

Channel	Expected Signal	Background	Observed
ee + Track (RunIIb)	0.5-2.1	1.0±0.3	0
ee + Track (RunIIa)	1.7-4.7	0.8±0.7	0
$\mu\mu$ + Track (RunIIa)	0.5-2.5	$0.3\pm^{1.3}_{0.3}$	2
$e\mu$ + Track (RunIIa)	2.0-2.6	0.9±0.4	0
$\mu^{\pm}\mu^{\pm}$ (RunIIa)	0.6-3.8	1.1±0.4	1

2 Supersymmetry searches

2.1 Chargino-Neutralino

In R-parity [a] conserving models of supersymmetry, the associated production of chargino and neutralino gives rise to a distinctive signature. The chargino ($\tilde{\chi}_1^{\pm}$) and neutralino($\tilde{\chi}_2^0$) each decay to leptons along with invisible particles ($\tilde{\chi}_1^{\pm} \to l^{\pm}\nu\tilde{\chi}_1^0$, $\tilde{\chi}_2^0 \to l^{\pm}l^{\mp}\tilde{\chi}_1^0$), giving a final state with three leptons and a momentum imbalance (missing E_T or $\not\!\!E_T$) in the detector.

CDF conducted a analysis which looked in five final states defined by purity of leptons used for the final states. Tight leptons have stricter selections and lower backgrounds, looser leptons are less pure, and tracks are simply charged particles. The results are summarized in Table 1. In this table lepton refers to electrons or muons. The final cross-section × branching ratio limits are shown in Figure 1. This analysis was performed with 2 fb^{-1}of data. It improves the CDF published limits [1]. Charginos with mass below 145 GeV/c^2 are excluded. These are first direct limits on mSUGRA chargino mass from the Tevatron.

DØ has added to their published result[2] an analysis which looks in the final state with two electrons and a track. The results are summarized in Table 2 and the limit is shown for an 'mSUGRA-inspired' scenario in Figure 2. The analyses performed by DØ used between 0.9 and 1.7 fb^{-1}. Charginos with mass below 145 GeV/c^2 are ruled out in this scenario.

2.2 Tau-sneutrino

Imposing R_P conservation is not necessary for supersymmetry. An analysis probing R_P violating SUSY is the DØ search for the superpartner to the tau-neutrino, the tau-sneutrino ($\tilde{\nu}_\tau$). The supersymmetric Lagrangian can then be modified to include terms such as

$$W_{RPV} = \frac{1}{2}\epsilon_{ab}\lambda_{ijk}L_i^a L_j^b E_k + \epsilon_{ab}\lambda'_{ijk}L_i^a Q_j^b D_k \quad (1)$$

[a] A multiplicative quantum number defined as $R_P = (-1)^{2S+3B+L}$.

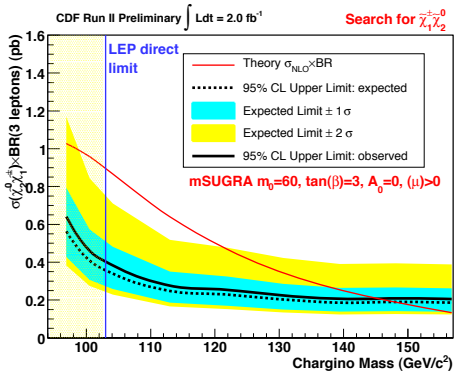

Figure 1: Figure shows the cross section × branching ratio limits from the CDF $\tilde{\chi}_1^{\pm}\tilde{\chi}_2^0$ search for the mSUGRA model. $\tilde{\chi}_1^{\pm}$ with mass below 145 GeV/c^2 is excluded.

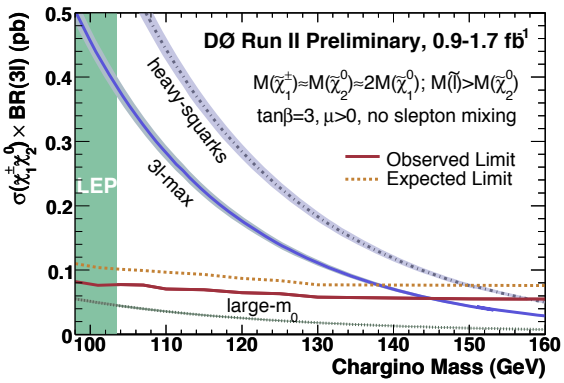

Figure 2: Figure shows the cross section × branching ratio limits from the DØ $\tilde{\chi}_1^{\pm}\tilde{\chi}_2^0$ search for an 'mSUGRA-inspired model'. $\tilde{\chi}_1^{\pm}$ with mass below 145 GeV/c^2 are excluded.

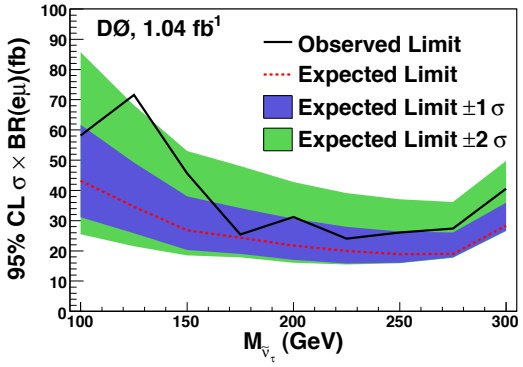

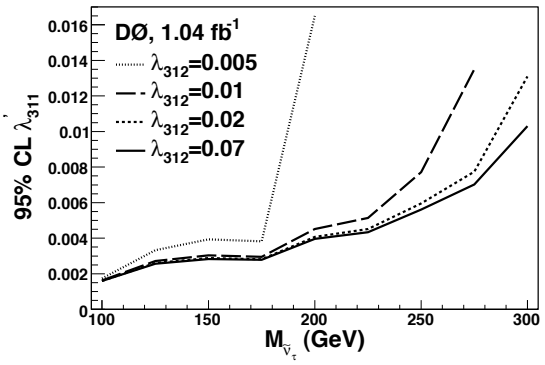

Figure 3: Figure shows the limits on the R_P violating couplings on the left side and cross section × branching ratio limits on the right from the DØ $\tilde{\nu}_\tau$ search as a function of the $\tilde{\nu}_\tau$ mass.

where the LLE and LQD terms represent lapton flavor violating interactions. The analysis is a direct search for resonant production of sneutrinos decaying into an electron and a muon performed under the hypothesis that the third-generation sneutrino ($\tilde{\nu}_\tau$) is the lightest supersymmetric particle and dominant, namely by assuming that all couplings but λ'_{311} and $\lambda_{312} = \lambda_{321}$ are zero. This analyses used 1 fb^{-1}of data to set limits on the R_P violating couplings as a function of $\tilde{\nu}_\tau$ mass. Figure 3 shows the limits.

3 Non-SUSY searches

3.1 Excited electrons

A possible way to explain the observed mass hierarchy of the three generations in the SM is compositeness. According to this approach, a quark or a lepton is a bound state of three fermions or of a fermion and a boson. DØ performs a search for an excited electron with 1 fb^{-1}of data. Single production of an excited electron (e^*) is considered in association with an electron via a four-fermion contact interactions, with the subsequent electroweak decay of the e^* into an electron and a photon. The $ee\gamma$ final state is fully reconstructable and nearly background-free. The selection is optimized for the mass of the e^* using two variables $\Delta R_{e\gamma}$ (separation between electron and photon) and $M_{e\gamma}$ (invariant mass of electron and photon). The limits on the cross section are shown in Figure 4. For the scale for contact interactions to be $\Lambda = 1$ TeV, excited electron masses below 756 GeV are excluded at the 95% C.L.

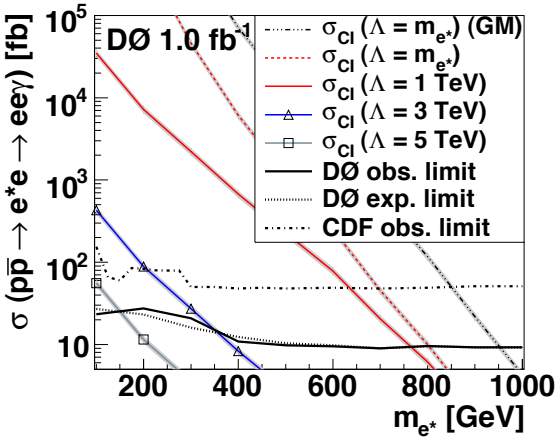

Figure 4: Figure shows the limits on the cross section × branching ratio of production of excited electron from a search performed at DØ . Experimental limits are compared to the contact interaction model prediction for different choices of Λ.

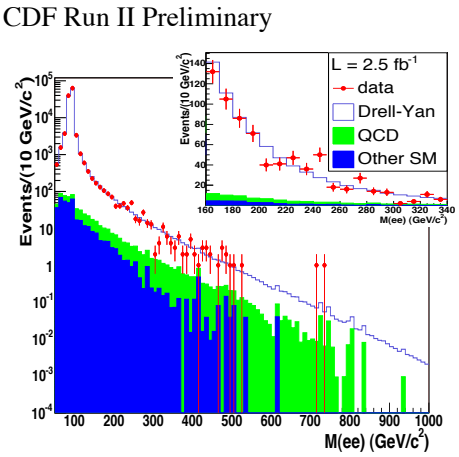

Figure 5: Figure shows the invariant mass distribution in the e^+e^- final state for the CDF Z' search. The most significant excess over standard model predictions is 3.8σ and occurs at 240 GeV/c^2 (shown in inset).

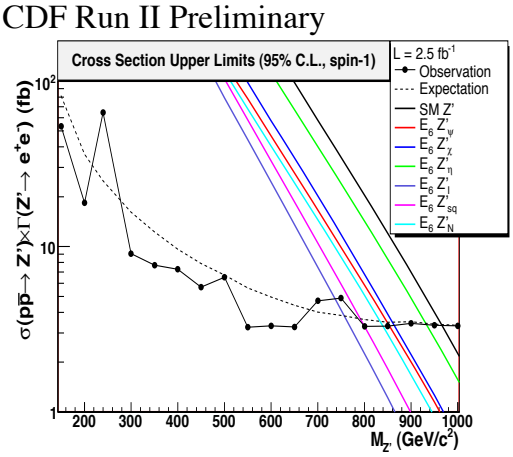

Figure 6: Figure shows the cross section limits on the Z' production from a CDF search. The different Z's are also shown. Standard model-like Z' with mass below 966 GeV/c^2 is excluded.

3.2 New gauge bosons

Search for Z'

The E6 model, which unifies the forces in the SM into a E6 gauge group, predicts the presence of additional neutral spin-1 bosons. These new bosons are referred to as Z's and they can mix with some arbitrary angle. Changing the value of the mixing angle used to benchmark the model gives the following six states : Z'_η, Z'_χ, Z'_ψ, Z'_I and Z'. The search based on 2.5 fb^{-1}and is carried out as a search for a narrow resonance in the dielectron (e^+e^-) final state with a mass range from 150 GeV/c^2 to 1050 GeV/c^2. The invariant mass distribution is shown in Figure 5 with the most significant excess (3.8σ) at 240 GeV/c^2 (inset).

Search for W'

Left-right-symmetric models, along with E6 models, also introduce additional gauge bosons. In the most general case, a new gauge group is comprised of a new mixing angle ζ, new couplings

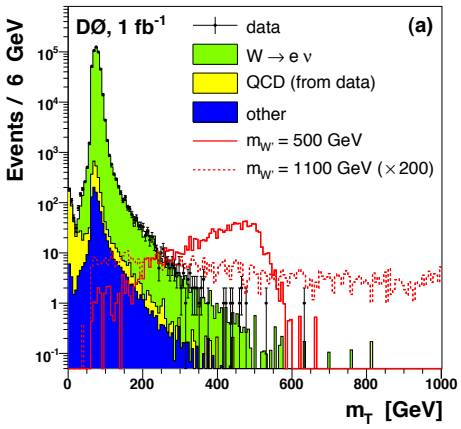

Figure 7: Figure shows the transverse mass (m_T) distribution in the $e\nu$ final state for the DØ W' search. The signal from a 500 GeV/c^2, and 1.1 TeV/c^2 W' boson is also shown..

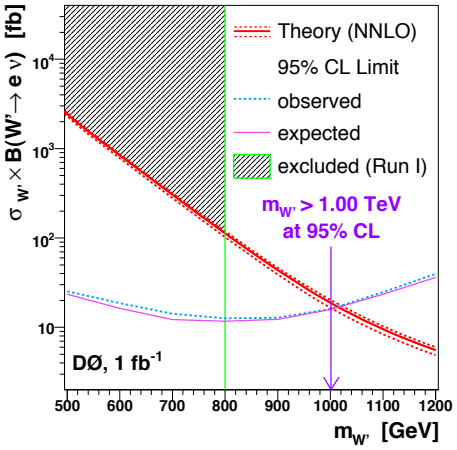

Figure 8: Figure shows the cross section limits on the W' production from a search at DØ . W' with standard model like couplings is ruled out below 1 TeV.

to fermions and a new CKM matrik U'. This analysis [3], based on 1 fb^{-1}, assumes no mixing, couplings equal to the SM couplings and the same CKM matrix as the SM. The width of the W' is assumed to scale with its mass, $m_{W'}$. The final state is an electron and a neutrino ($W' \to e\nu$). The transverse mass (m_T) of the electron and neutrino is constructed, and the tail of the m_T distribution is searched for possible excesses. Figure 7 shows the m_T distribution with signal shown for two possible masses of the W'. Figure 8 shows the cross section × branching ratio limits on W' production. A W' boson with mass below 1 TeV is ruled out at 95% C.L.

4 Conclusions

CDF and DØ have searched for new physics in lepton final states with more than 2 fb^{-1}. The leptonic final states provide a rich set for searches for physics beyond the standard model. No signs of new physics have been found yet, but new constraints have been set on new-physics models. With the improving Tevatron performance and optimal working of the two experiments, next year will push the boundaries of physics even further.

References

1. Search for Chargino-Neutralino Production in $p\overline{p}$ Collisions at $\sqrt{s} = 1.96$ TeV, T. Aaltonen *et al*, *Phys. Rev. Lett.* **99**, 191806 (2007)
2. Search for Supersymmetry via Associated Production of Charginos and Neutralinos in Final States with Three Leptons, V. Abazov *et al*, *Phys. Rev. Lett.* **95**, 151805 (2005)
3. Search for W' Bosons Decaying to an Electron and a Neutrino with the D0 Detector , V. Abazov *et al*, *Phys. Rev. Lett.* **100**, 031804 (2008)
4. CDF collaboration , http://www-cdf.fnal.gov/physics/exotic/exotic.html
5. DØ collaboration, http://www-d0.fnal.gov/Run2Physics/WWW/results/np.htm

MODULI, ANOMALOUS U(1) AND LHC PHENOMENOLOGY

E. DUDAS[1,2], Y. MAMBRINI[2], S. POKORSKI[3], A. ROMAGNONI[2,1]
[1] *CPhT, Ecole Polytechnique 91128 Palaiseau Cedex, France*
[2] *Laboratoire de Physique Théorique, Université Paris-Sud, F-91405 Orsay, France*
[3] *Institute of Theoretical Physics, Warsaw University, Hoza 69, 00-681 Warsaw, Poland*

In these proceedings we present a phenomenological model of moduli stabilization where the uplift of the cosmological constant to zero is provided by a Fayet-Iliopoulos sector. In the presence of an extra anomalous U(1) gauge symmetry, fields with the same features of the "messengers" in gauge-mediation scenarios are naturally introduced. The original phenomenology induced at low-energy in this kind of mixed gravity-gauge mediation presents a superpartners spectrum efficiently compressed and a good dark matter relic density compatible with WMAP bounds.

1 Introduction

A quite general result concerning the high-energy models in the presence of extra-dimensions, it's that when one reduces to the four dimensional space time, new fields appear in the model, often parametrizing flat directions. This kind of fields are called moduli. For example, in the following, the modulus T will be the superfield representing the fluctuations of the overall internal volume. Since the vev of the moduli are strictly related to physical parameters, it is compelling to find a mechanism to provide them a potential in order to properly define a minimum.
Recently, Kachru et al. [1] (KKLT) proposed a strategy to stabilize the moduli in the context of Type IIB string theory orientifold, following earlier work [2]. The KKLT set-up involves different logical steps to achieve a supersymmetry breaking Minkowski vacuum, while stabilizing all moduli. All steps except the last one (uplifting the vacuum energy through the addition of anti D3-branes) can be understood within the context of an effective supergravity. Other works changed this point by insisting on the possibility of using F-terms or D-terms of matter fields in a decoupled sector to perform the uplift. In this proceedings we will show an alternative way to obtain de Sitter space with a TeV gravitino mass by using a Fayet-Iliopoulos (FI) model as uplift sector [3].

It is important to stress that this kind of approach is not an attempt to solve the problem of the cosmological constant, but instead it is meant to be a pragmatic program: The aim is to look at the low-energy phenomenology starting from a high-energy model, imposing some constraints due to consistency requirements and fixing some basic phenomenological inputs (like $\Lambda_c = 0$ and the value of the mass of the gravitino).
The peculiarity of our model is due to the presence of one extra $\mathrm{U}(1)_X$ gauge symmetry in the game. This kind of symmetry appears in a very natural way in many compactification of extra-dimensional models, and in the most general case, all the fields entering in the stabilization and uplifting procedure can be charged under it.
More precisely the $\mathrm{U}(1)_X$ transformations for the gauge superfield V_X, the matter chiral superfields Φ_i and the modulus T have the form:

$$\delta V_X \;=\; \Lambda_X + \bar{\Lambda}_X \quad , \quad \delta\Phi_i \;=\; -2q_i\Phi_i\Lambda_X \;, \qquad \delta T \;=\; \delta_{GS}\Lambda_X \;, \tag{1}$$

where q_i are the charges of the fields Φ_i and δ_{GS} a suitable constant. Gauge invariance forces the Kahler potential for the modulus T to be of the form $K(T + \bar{T} - \delta_{GS}V_X)$ and this leads in turn to the FI term

$$\xi_{FI} \;=\; \frac{3\delta_{GS}}{2}\frac{1}{T+\bar{T}} \;\; . \tag{2}$$

The presence of this T-dependent FI term is crucial, because the corresponding non-vanishing D-term, even if it doesn't change directly the cosmological constant, at the same time induces the suitable F-terms performing the uplift and play an important role for the corresponding low-energy phenomenology.

2 Uplifting and Gravity mediation

2.1 The model

The supergravity model we focus on, is defined in terms of the modulus T and two scalar fields $\Phi_\pm$ of opposite charges under $\mathrm{U}(1)_X$, by the superpotential:

$$W \;=\; W_0 \;+ m\;\phi_+\phi_- + a\;\phi_-^q\;e^{-bT} \;. \tag{3}$$

In the presence of a charged modulus T, the last term in Eq. 3 is the right gauge invariant version of the KKLT gaugino condensation contribution to the superpotential. The usual negative W_0 constant, the presence of the charged fields $\Phi_\pm$, their mass term and the interaction term between T and Φ_-, are motivated by stringy argument and can be microscopically defined in the type IIB orientifold setup, in terms of fluxes, intersecting branes and stringy instantons effects.

Using a conventional Kahler potential of the form [a] $K = |\phi_+|^2 + |\phi_-|^2 - 3\ln(T+\overline{T})$ and considering a region of the parameters space where

$$\delta_{GS} \;\sim\; 1 \quad , \quad m \ll M_P \quad , \quad W_0 \ll M_P^3 \quad , \quad a\;e^{-bT} \;\ll\; W_0 \;\ll m \tag{4}$$

hold, the minimization of the scalar potential given by standard supergravity formula in terms of the auxiliary fields [b] F_i and D

$$V(\phi_+,\phi_-,T) = F^T F_T + F^- F_- + F^+ F_+ + \frac{g_X^2}{2}D^2 - 3e^K|W|^2 \tag{5}$$

[a] The Kahler metric of the charged fields $\Phi_\pm$ can be more complicated and can also depend on T. We checked explicitly that with the Kahler potential $K = -3\ln(T+\bar{T}-|\Phi_-|^2-|\Phi_+|^2)$ we obtain very similar results.

[b] Here we use the definitions $F_i = e^{K/2}D_iW$ and $D = K_+\Phi_+ - K_-\Phi_- + \xi_{FI}$. As usual, the indices are raised and lowered by using the Kahler metric.

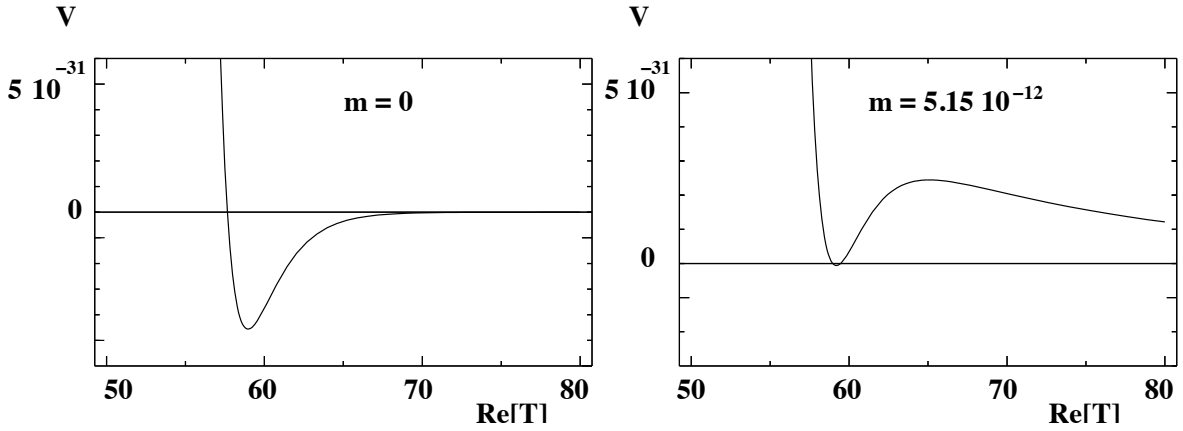

Figure 1: Scalar potential (in M_P units) for $m = 0$ (left) and $m \neq 0$ (right) for a gravitino mass of 3.3 TeV. The other parameters are determined by gauge invariance conditions, minimization of the potential and $\Lambda_c = 0$.

shows that the vacuum of the theory breaks supersymmetry. Moreover it can give a zero cosmological constant Λ_c if the parameters m and W_0 satisfy $|m\phi_-| \simeq \sqrt{3}\,|W_0|$, considering that the vev of Φ_- is fixed proportional to ξ_{FI} by the FI mechanism. In Fig. 1 we show the shape of the scalar potential in the two cases $m = 0$ and m tuned in order to have $\Lambda_c = 0$. In our case the uplift of the AdS to a Minkowski vacuum is mainly provided by F_+, but the crucial point is that this is induced by the non-vanishing D-term. Moreover, since the superpotential for T is not completely decoupled from the supersymmetry breaking sector, due to the interaction term with Φ_-, F_T is bigger than the values obtained in typical sequestered F-term uplifting models, even if the numerical value for T is very close to its supersymmetric solution.

2.2 First phenomenological results

Even if the supersymmetry is broken in a hidden sector, (super)gravity interactions communicate this breaking to the observable sector, that we take for simplicity to be the Minimal Supersymmetric Standard Model (MSSM). In particular, irrespective on the string theory brane configuration giving our model as effective field theory, if magnetic fluxes are turned on, the coupling constants of the MSSM gauge fields contain a T-dependence. This implies that under very general assumptions, a mass for the gaugino fields is directly provided,and it as the form

$$(M_a)_{\rm grav.} \simeq \frac{F^T}{T}\ . \tag{6}$$

Concerning the scalars soft masses, the relevant quantity for computing the soft terms is the coupling of the matter fields metric $K_{i\bar{j}}$ to the SUSY breaking fields. This can in turn be parameterized as

$$K_{i\bar{j}} = (T+\overline{T})^{n_i}\left[\delta_{i\bar{j}} + (T+\overline{T})^{m_{ij}}|\phi_+|^2 Z'_{i\bar{j}} + (T+\overline{T})^{p_{ij}}|\phi_-|^2 Z''_{i\bar{j}} \right.$$
$$\left. +(T+\overline{T})^{l_{ij}}(\phi_+\phi_- Z'''_{i\bar{j}} + \text{h.c}) + O(|\phi_i|^4)\right], \tag{7}$$

but the final results is quite simple:

$$(\tilde{m}^2_{0\ i\bar{j}})_{\rm grav.} = m^2_{3/2}\left[\delta_{i\bar{j}} + (\ldots)\right]. \tag{8}$$

Here $(\ldots)$ represents subleading terms if the weights n_i and m_{ij} satisfy the relation $r_{ij} = m_{ij} + (n_i - n_j)/2 \leq -1$. Actually this relation is strongly motivated from the string theory point of view, and the only dangerous case is $r_{ij} = 0$, where a flavour dependence and FCNC

effects could arise.
The first important result is that in our non completely decoupled model, F^T is greater than the usual KKLT-like models and we obtain a splitting between the scalar and gaugino masses smaller by a factor of two. Nonetheless this implies that the one-loop contributions (AMSB) are less important here compared to the tree-level ones.
Finally, in the presence of gravity mediation, trilinear couplings are produced in a similar way and the μ and B_μ parameters for the Higgs sector can be generated at the TeV scale through a Giudice-Masiero mechanism [4].

3 Anomalies and Mixed mediation

3.1 Anomalies and messengers

As introduced in the previous section, the T-modulus transforms under the extra anomalous $\mathrm{U}(1)_X$. Moreover, in a very generic way, it is related to the MSSM gauge coupling via a dependence on T of the gauge kinetic functions. Therefore this implies that under $\mathrm{U}(1)_X$ gauge transformation, mixed $\mathrm{U}(1)_X$ - G_a^2 anomalous terms are produced (with G_a subgroup of the SM gauge group) and a chiral spectrum is required. More precisely, there should be fields carrying Standard Model quantum numbers charged under the additional $\mathrm{U}(1)_X$.
Since quarks and leptons carrying $\mathrm{U}(1)_X$ charge should imply various phenomenological problems (related to very large soft masses), the most natural possibility is to keep uncharged under $\mathrm{U}(1)_X$ the SM fields and to introduce additional heavy fields with the right quantum numbers. These fields have exactly the features of the "messengers" fields in gauge-mediated scenario [5] (GMSB).
Since the cancelation of the anomaly implies a positive $\mathrm{U}(1)_X$ charge for the messengers [c] M and $\tilde{M}$, a natural gauge invariant superpotential is

$$W_{\mathrm{mess}} = \lambda \phi_- M \tilde{M} \ , \tag{9}$$

which naturally pushes the messenger scale up to the GUT scale.
In the usual gauge mediated scenario, adding messengers to a supersymmetry breaking sector generates a new supersymmetric vacuum. However, in our case, the vacuum presented in the previous section is preserved by $\mathrm{U}(1)_X$.
Nonetheless another very important new point with respect to the standard gauge-mediation concerns the contribution to the scalar masses. Indeed, as pointed out by Poppitz and Trivedi [6], when the supertrace of the messenger mass matrix is non-vanishing, a new UV divergent term appear at the quantum level and play a very crucial role in what follows.
More precisely, in our case the supertrace is proportional to the $\mathrm{U}(1)_X$ D-term:

$$(StrM^2)_{\mathrm{mess.}} \ = \ 2 \ g_X^2 \ D \ = \ \frac{2m^2}{\left(T+\bar{T}\right)^3} \ \neq \ 0 \ . \tag{10}$$

While this does not affect the GMSB one-loop contribution for the gaugino masses,

$$M_a^{\mathrm{GMSB}} \simeq \frac{m}{\left(T+\bar{T}\right)^{3/2}} \frac{g_a^2}{16\pi^2} \left(\frac{\phi_+}{\phi_-}\right) \ , \tag{11}$$

it changes significantly the two-loop soft masses for the scalar superpartners

$$(\tilde{m}_0^{\mathrm{GMSB}})^2 \simeq \frac{m^2}{\left(T+\bar{T}\right)^3} \sum_a \frac{g_a^4}{128\pi^4} C_a \left[1 - \log\left(\frac{\Lambda_{\mathrm{UV}}}{\lambda\phi_-}\right)^2 + \left(\frac{\phi_+}{\phi_-}\right)^2\right] \ , \tag{12}$$

[c] The messengers fields are chosen in a complete vector-like SU(5) in order to preserve the perturbative gauge coupling unification.

Table 1: Low energy sample spectra for two different choices of the high-energy parameters, in both the cases of simple gravity and mixed gravity-gauge mediation. All superpartner masses are in GeV, whereas W_0, m and t are in Planck units. The last line correspond to the relic abundance, within WMAP bounds in each case.

	(A) Gravity	**(A) Mixed**	**(B) Gravity**	**(B) Mixed**
W_0	$-7\ 10^{-13}$	$-7\ 10^{-13}$	$-4.3\ 10^{-13}$	$-4.3\ 10^{-13}$
m	$7.3\ 10^{-12}$	$7.3\ 10^{-12}$	$3.1\ 10^{-12}$	$3.1\ 10^{-12}$
a	1	1	1	1
b	0.3	0.3	0.5	0.5
q	1	1	1	1
$\tan\beta$	30	30	15	15
t	97.3	97.3	60.2	60.2
λ	0	$1.7\ 10^{-3}$	0	$1.1\ 10^{-3}$
N_{Mess}	0	6	0	6
μ (GeV)	810	186	1070	216
$B\mu\ (GeV)^2$	$(400)^2$	$(330)^2$	$(870)^2$	$(730)^2$
$m_{\chi_1^0}$	110	120	140	150
$m_{\chi_1^+}$	220	160	290	200
$m_{\tilde{g}}$	760	850	950	1060
m_h	120	120	120	120
m_A	2220	1740	3290	2770
$m_{\tilde{t}_1}$	1380	990	1770	1220
$m_{\tilde{t}_2}$	1920	1280	2610	1710
$m_{\tilde{c}_1},\ m_{\tilde{u}_1}$	2580	1950	3300	2420
$m_{\tilde{b}_1}$	1910	1250	2610	1700
$m_{\tilde{b}_2}$	2310	1930	3230	2690
$m_{\tilde{s}_1},\ m_{\tilde{d}_1}$	2580	1950	3300	2420
$m_{\tilde{\tau}_1}$	2290	2130	3200	2870
$m_{\tilde{\tau}_2}$	2420	2160	3230	2960
$m_{\tilde{\mu}_1},\ m_{\tilde{e}_1}$	2550	2290	3270	2910
Ωh^2	–	0.12	–	0.12

where C_a is the Casimir in the MSSM scalar fields representations. From a low energy - GMSB point of view, the logarithmic divergence shows the scale beyond which "new physics" occurs, since there the scalars can become tachyonic. In our case, we can take Λ_{UV} as the Planck scale, and for suitable values of λ the GMSB contribution is actually negative.

3.2 Phenomenology

Once the messengers are introduced in the model, in the complete framework scalar and gaugino masses get contributions both from gravity and gauge mediation diagrams

$$\begin{aligned}(\tilde{m}_0^2) &= (\tilde{m}_0^2)_{\mathrm{grav.}} + N_{\mathrm{Mess}}(\tilde{m}_0^{\mathrm{GMSB}})^2\ ,\\ M_a &= (M_a)_{\mathrm{grav.}} + N_{\mathrm{Mess}}(M_a^{\mathrm{GMSB}})\ .\end{aligned} \tag{13}$$

The negative contibution to $\tilde{m}_0^2$ induced by the UV divergence has strong consequences on the mass spectrum and the phenomenology of the model. Indeed, first of all, the spectrum is generically "compressed", since the values of the gaugino masses are increased whereas the

scalars ones decreased. Moreover, since the GMSB negative contributions are proportional to the SM charges of the scalars, the squarks are more sensitive than sleptons to them, whereas the gravitational contribution is universal, as shown above. The result of this interplay is shown in Table 1, where two different point in the space of the high-energy parameters are chosen (together with the value of the coupling λ and the number of messengers $N_{\rm Mess}$) and the comparison between the simple gravity mediated model and the complete one is shown. The low-energy mass spectrum is calculated using the Fortran package `SUSPECT` [7].
In addition, also the nature of the neutralino is considerably altered. Indeed, decreasing the value of m^2_{U3} and m^2_{Q3} affects the RG equation for $m^2_{H_2}$ and consequently one can have a smaller value for μ^2. In this case the lightest neutralino is generally higgsino-like or a mixed bino-higgsino state and a good value for the relic abundance, compatible with WMAP bounds, is obtained, whereas this is not possible in the simple gravity mediated models, as computed using the routines provided by the program `micrOMEGAs2.0` [8].

Acknowledgments

Work partially supported by the CNRS PICS # 2530 and 3059, RTN contracts MRTN-CT-2004-005104 and MRTN-CT-2004-503369, the European Union Excellence Grant, MEXT-CT-2003-509661 and the European contract MTKD-CT-2005-029466. E.D. would like to thanks the financial support via the "Marie Curie Host Fellowship for Transfer of Knowledge" MTKD-CT-2005-029466. The work of Y.M. is sponsored by the PAI program PICASSO under contract PAI–10825VF. He would like to thank the European Network of Theoretical Astroparticle Physics ILIAS/N6 under contract number RII3-CT-2004-506222 and the French ANR project PHYS@COLCOS for financial support. The work of A.R. was partially supported by INFN and by the European Commission Marie Curie Intra-European Fellowships under the contract N 041443.

References

1. S. Kachru, R. Kallosh, A. Linde and S. P. Trivedi, *Phys. Rev.* D **68** (2003) 046005 [arXiv:hep-th/0301240].
2. S. B. Giddings, S. Kachru and J. Polchinski, *Phys. Rev.* D **66** (2002) 106006 [arXiv:hep-th/0105097].
3. E. Dudas, Y. Mambrini, S. Pokorski and A. Romagnoni, *JHEP* **0804** (2008) 015 [arXiv:0711.4934 [hep-th]].
4. G. F. Giudice and A. Masiero, *Phys. Lett.* B **206** (1988) 480.
5. G. F. Giudice and R. Rattazzi, *Phys. Rept.* **322** (1999) 419 [arXiv:hep-ph/9801271].
6. E. Poppitz and S. P. Trivedi, *Phys. Lett.* B **401** (1997) 38 [arXiv:hep-ph/9703246].
7. A. Djouadi, J. L. Kneur and G. Moultaka, *Comput. Phys. Commun.* **176** (2007) 426 [arXiv:hep-ph/0211331].
8. G. Belanger, F. Boudjema, A. Pukhov and A. Semenov, *Comput. Phys. Commun.* **176** (2007) 367 [arXiv:hep-ph/0607059] ;
   See also the web page http://wwwlapp.in2p3.fr/lapth/micromegas .

MODEL-DEPENDENT SEARCHES FOR NEW PHYSICS AT HERA

G. BARBAGLI
on behalf of the H1 and ZEUS Collaborations
INFN Firenze, Via G. Sansone 1, 50019, Sesto Fiorentino (FI), Italy

Some of the searches for phenomena and particles beyond the Standard Model performed at HERA relying on specific theoretical models and using almost all the collected luminosity are discussed here. They particularly concern leptoquarks, lepton flavour violation, excited fermions, the anomalous top coupling and contact interactions, with improved limits on the quark radius.

1 Introduction

The HERA collider delivered luminosity for 15 years colliding e^+ (e^-) with p at a centre-of-mass energy $\sqrt{s} \simeq$ 300-320 GeV. The data taking started in 1992 and continued until 2000 (HERA I phase). Then a substantial upgrade program involved both the machine and the experiments and the data taking was resumed in 2003 and continued until 2007 (HERA II phase), during which longitudinally polarised $e^{\pm}$ were available in most of data. The two general purpose experiments H1 and ZEUS ended data taking in summer 2007, after collecting a total integrated luminosity of about 1 fb^{-1}. At HERA an extensive program of searches for new particles and phenomena beyond the Standard Model (SM) has been carried out in a unique ep environment. The focus in this paper will be on recent results of searches inspired or driven by specific theoretical models.

2 Leptoquarks

Starting from the symmetry between the quark and the lepton sectors many extensions of the SM predict bosons with fractional electromagnetic charge and both lepton and baryon numbers. A widely used model for leptoquarks is the phenomenological model of Buchmüller-Rückl-Wyler (BRW) [1] which assumes invariance under $SU(3)_C \times SU(2)_L \times U(1)_Y$, conservation of the lepton number L and the baryon number B and a set of 7 scalar and 7 vector leptoquarks (4 decaying into both eq and νq) classified according to the fermion number $F = 3B + L = 0, 2$ and coupling to either left handed or right handed leptons, but not to both, with fixed branching ratio into $e\nu$ (1, 1/2), νq (0, 1/2). At HERA, leptoquarks can be resonantly produced in the s channel or exchanged in the u channel between the incoming lepton and the quark from the proton. The resonant production shows up as a peak in the mass spectrum or an enhancement in x distribution at the value corresponding to the mass M of the leptoquark: $x = M^2/s$. As a consequence of quark densities in the proton, e^-p and e^+p collisions offer respectively best sensitivities to $F = 2$ and $F = 0$ leptoquarks.
The availability of polarisation of both signs within the HERA II sample has the advantage of enhancing the sensitivity to individual leptoquarks species. H1 searched for leptoquarks

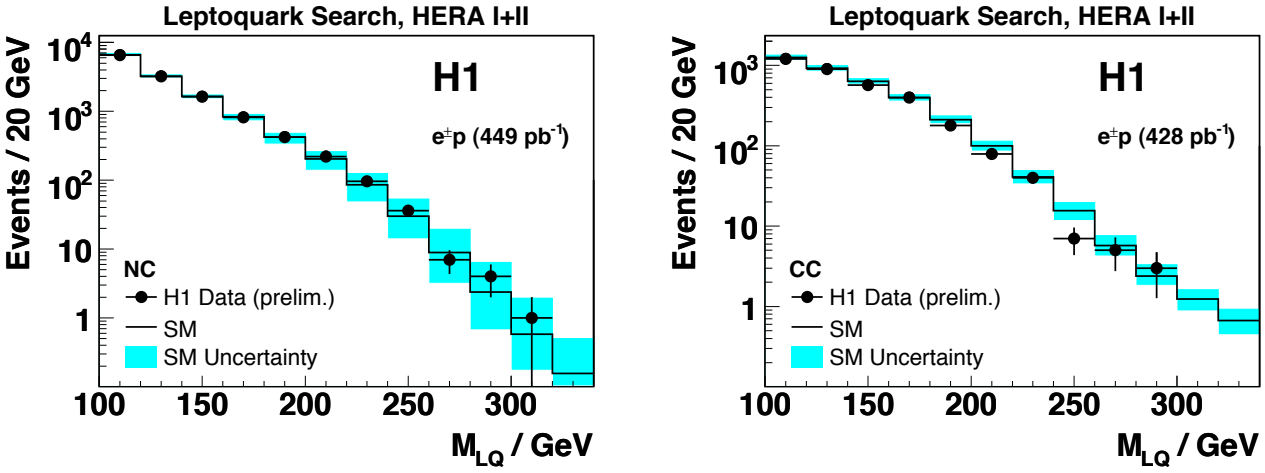

Figure 1: Mass spectra of HERA I + II $e^{\pm}p$ data for Neutral Current (left) and Charged Current (right) events in the H1 leptoquark search. Data points are compared to Standard Model (SM) expectations.

studying the inclusive Neutral Current and Charged Current Deep Inelastic Scattering high Q^2 $e^{\pm}p$ samples from HERA I and HERA II and using an integrated luminosity of 482 pb^{-1}.

No excess was seen in the $e-jet$, $\nu-jet$ mass spectra (fig. 1) and limits were set on the couplings and masses of the different leptoquark types [2] (fig. 2).

3 Lepton Flavour Violation

Leptoquarks can couple to different fermion generations and mediate lepton flavour violation processes in family non diagonal models.
H1 searched for $F = 2$ leptoquarks coupling to eq and μq using $e^{-}p$ HERA II data and an integrated luminosity of 158 pb^{-1}. No evidence for leptoquarks mediating lepton flavour violation was obtained and limits were set on couplings and masses of leptoquarks coupling to 1st and 2nd generation fermions (fig. 2). For an electromagnetic type coupling masses below 291-433 GeV can be excluded depending on the leptoquark type [3].

4 Excited leptons

To try to explain the hierarchy problem, models of compositeness introduce substructures to SM fermions, implying the existence of fermion excited states. Couplings between excited fermions and SM fermions can be described with phenomenological gauge mediated models [4,?,?]. Excited fermion states have spin and isospin 1/2 with both left-handed (F_L^*) and right-handed (F_R^*) components in weak iso-doublets. They can decay into fermions and gauge bosons. Magnetic type transitions between SM fermions F and excited states F^* can take place. Weight factors f, f' and f_s are used to set the coupling strength to the three gauge groups (U(1), SU(2) and SU(3)) . The branching ratios of excited lepton decays can be fixed by assuming a specific relation between f and f' and then the production cross section depends only on f/Λ where Λ is the compositeness scale.

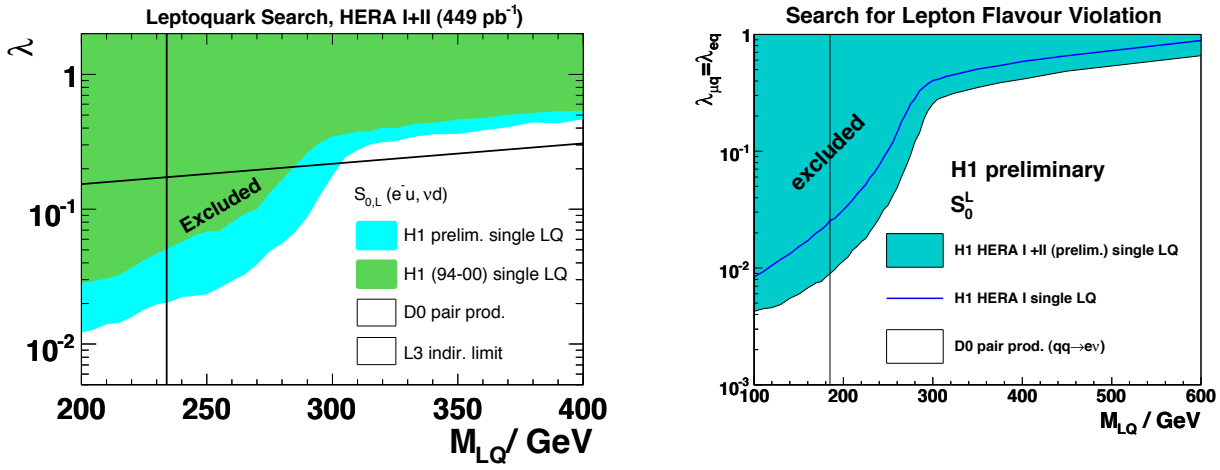

Figure 2: H1 exclusion limits at 95 % C.L. on the coupling λ as a function of the mass for the scalar leptoquark coupling to the first generation S_L^0 (left). H1 exclusion limits at 95 % C.L. on the coupling $\lambda_{\mu q} = \lambda_{eq}$ as a function of the mass for the scalar leptoquark mediating lepton flavour violation S_L^0 (right).

H1 searched for $e^* \to e\gamma$, $e^* \to eZ$ with $Z \to q\bar{q}$, and $e^* \to \nu W$ with $W \to qq'$ using $e^{\pm}p$ data and an integrated luminosity of 475 pb^{-1}. No evidence for e^* production was observed. Improved limits with respect to LEP and Tevatron were set [7].

Due to the helicity structure of electroweak interactions and the valence quark densities in the proton, signals for excited neutrinos are expected to be stronger in e^-p rather than in e^+p data. H1 searched for $\nu^* \to \nu\gamma$, $\nu^* \to \nu Z$ with $Z \to q\bar{q}$, and $\nu^* \to eW$ with $W \to qq'$ using e^-p data and an integrated luminosity of 184 pb^{-1}. No evidence was found and new limits were set [8](fig. **??**). Masses were excluded in the range up to 213 GeV ($f = -f'$) and 196 GeV ($f = f'$). The H1 analysis has entered regions of masses not previously explored.

5 Anomalous top coupling

At HERA top quarks can only be singly produced. SM single-top production proceeds via the Charged Current reaction $ep \to \nu t\bar{b}$X. As the SM cross section at HERA is less than 1 fb any observed single-top event must come from physics beyond the SM. In a Flavour Changing Neutral Current reaction the incoming lepton exchanges a γ or Z with an up-type quark in the proton, yielding a top quark in the final state most sensitive to a coupling of the type $tq\gamma$. The u-quark dominates at large x and therefore the production of single top quark is related to the coupling $tu\gamma$. H1 searched for single top events in a sample of isolated leptons with high p_t using $e^{\pm}p$ data and an integrated luminosity of 482 pb^{-1}. The analysis searched for anomalous production of t decaying into b and W with subsequent decay of W into an electron or a muon. A multivariate discrimination, based on a phase space density estimator with a range searching algorithm was used to separate the signal from the SM background (mostly real W production). The upper limit on the cross section set by H1 [9] is $\sigma_{ep\to etX} < 0.16$ pb, leading to the most stringent limit to date on $k_{tu\gamma}$ <0.14 at 95 % C.L. (fig.4).

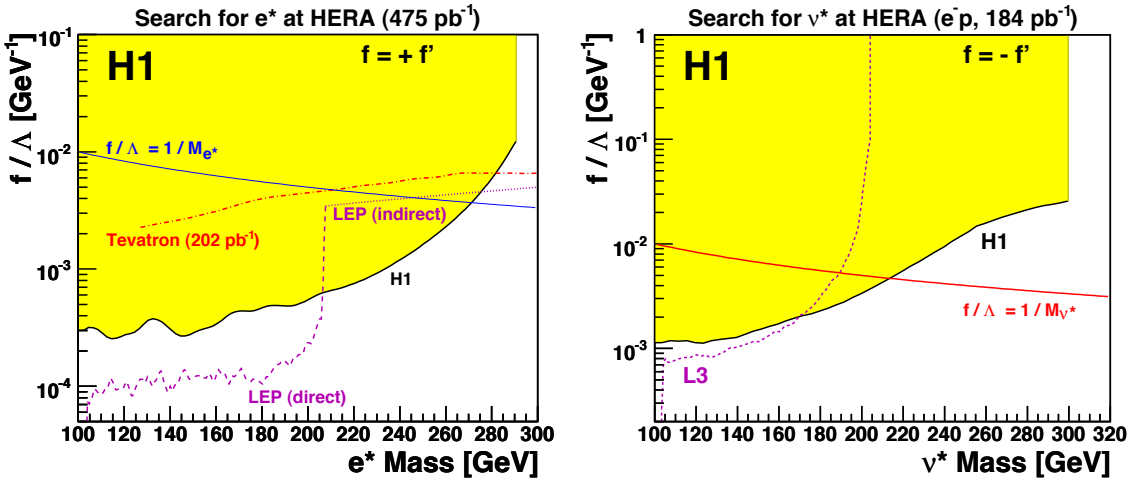

Figure 3: H1 exclusion limits at 95 % C.L. on the coupling f/Λ as a function of the mass of the e^* for gauge mediated interactions, with the assumption $f = +f'$ (left). H1 exclusion limits at 95 % C.L. on the coupling f/Λ as a function of the mass of the ν^* assuming $f = -f'$ (right).

6 Contact interactions and quark radius

Four-fermion contact interactions describe effects from processes at much higher scales, which could alter the SM distributions at high Q^2 and interfere with the predictions at intermediate Q^2. These effects modify the tree level amplitude $eq \rightarrow eq$. Let us focus on vector terms (as scalar and tensor terms are already costrained by previous searches). The Lagrangian can be written as:

$$L_{CI} = \sum_{\alpha,\beta=L,R}^{q=u,d} \eta^q_{\alpha\beta}(\bar{e}_\alpha \gamma^\mu e_\alpha)(\bar{q}_\beta \gamma_\mu q_\beta) \quad (1)$$

The equation:

$$\eta_{\alpha\beta} = \epsilon \frac{g^2_{CI}}{\Lambda^2} \quad (2)$$

where $g_{CI} = 4\pi$ $\epsilon = \pm 1$ defines the structure of the model.

Contact interaction effects could come from the exchange of extra gauge bosons (Z'), the production or exchange of leptoquarks or squarks, compositeness, gravitational effects (extra-dimensions) or from a finite quark radius.

ZEUS analysed inclusive Neutral Current Deep Inelastic $e^{\pm}p$ data from HERA I and HERA II corresponding to an integrated luminosity of 330 pb^{-1}, comparing the data to SM predictions and performing a QCD fit where experimental and theoretical uncertainties are taken into account [10]. Besides general model independent limits on contact interactions (values of the scale Λ_{eeqq} in the range 2.0-8.0 TeV) depending on the chiral structure, limits were also set on the heavy leptoquark (beyond the available CM energy) couplings to the first generation (M_{LQ}/λ in the range 0.29-2.08 TeV).

In some $4+n$ dimensional string theories [11,12,13] compactified extra dimensions have size $R \simeq 1$ mm. The effective Planck scale M_S related to the Planck scale $M_P \simeq 10^{19}$ GeV: $M_P^2 = M_S^{2+n} R^n$ can be as small as 1 TeV. Graviton can propagate into the extra dimension, visible in the or-

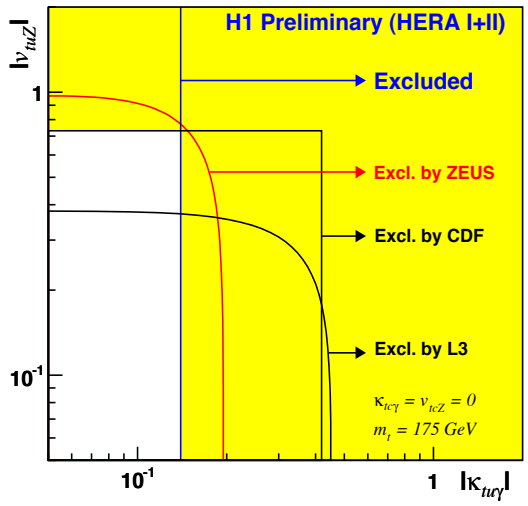

Figure 4: Exclusion limits at 95 % C.L. on the anomalous top coupling $k_{tu\gamma}$ from H1 and ZEUS compared to limits from LEP and Tevatron (anomalous couplings to charm are neglected, the top mass is set to 175 GeV).

dinary 4 dimensions as a Kaluza-Klein tower of excited states with spacing $\Delta m = \frac{1}{R}$. Such states can be summed up to M_S, give sizeable effects, equivalent to a contact interaction term $\eta^G \simeq \frac{\pm\lambda}{M_S^4}$ where $\lambda \simeq 1$ [14]. The interference with the SM can be constructive or destructive.
Constraints were derived by ZEUS for such extra dimension scales: $M_S > 0.9$ TeV for $\lambda = -1$ and $M_S > 0.88$ TeV for $\lambda = +1$.
As far as the finite size of the quark is concerned in a classical approach to the quark substructure a charge distribution of radius R_q in the quark can be described using a form factor:

$$\frac{d\sigma}{dQ^2} = \frac{d\sigma^{SM}}{dQ^2} \cdot (1 - \frac{R_q^2}{6} \cdot Q^2)^2) \tag{3}$$

This effect leads to a decrease of cross sections at high Q^2. An upper limit on quark radius was extracted from the ZEUS analysis: $R_q < 0.62 \cdot 10^{-16}$ cm. A study of high Q^2 Neutral Currents single differential cross section by H1 using the complete HERA I and HERA II data and an integrated luminosity of 270 pb^{-1} (e^+p) and 165 pb^{-1} (e^-p) [15] led to a limit: $R_q < 0.74 \cdot 10^{-16}$ cm at 95 % C.L. (fig. 5).

7 Conclusions

The complete statistics of 15 years of data taking is being exploited by H1 and ZEUS to improve the sensitivity of the searches for new physics in the unique HERA environment. H1 and ZEUS at HERA have performed a number of model dependent searches finding no evidence for leptoquarks or lepton flavor violation, for excited electrons or excited neutrinos. Looking for single top production new limits on the anomalous top coupling are set. Limits on the contact interaction scales and quark radius have been updated fitting the Deep Inelastic Scattering

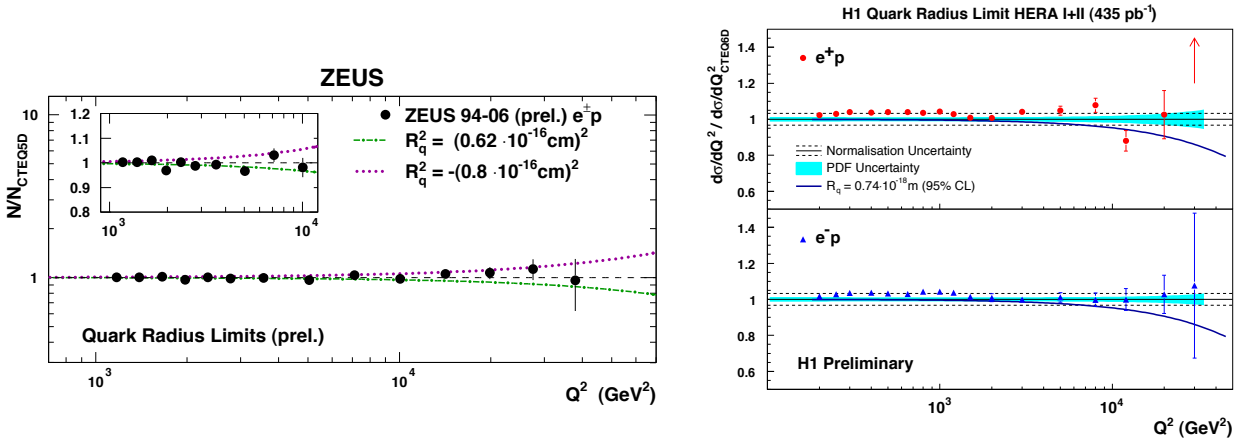

Figure 5: Ratio of inclusive neutral current deep inelastic scattering data obtained by ZEUS in $e^{\pm}$ (left) and single differential cross sections obtained by H1 in e^+p (top right) e^-p (bottom right) to SM expectations as a function of Q^2, compared with 95 % C.L. limits on the effective mean square radius of the electroweak charge of the quark.

differential cross sections at high Q^2. For some of these searches the two collaborations are going to provide a combination of H1 and ZEUS data.

References

1. W. Buchmuller, R. Ruckl and D. Wyler *Phys. Lett.* B **191**, 442 (1987). W. Buchmuller, R. Ruckl and D. Wyler *Phys. Lett.* B **448**, 320 (1987).
2. H1 Collaboration, Contributed paper to DIS08 H1prelim-07-164 and references therein.
3. H1 Collaboration, Contributed paper to DIS08 H1prelim-07-167 and references therein.
4. K.Hagiwara, S. Komamiya and D.Zeppenfeld, *Z. Phys.* C **29**, 115 (1985).
5. U.Baur, M.Spiras and P.M. Zerwas, *Phys. Rev.* D **42**, 815 (1990).
6. F. Boudjema, A. Djouadi and J.L. Kneur, *Z. Phys.* C **57**, 425 (1993).
7. F.D. Aron *et al.* [H1 Collaboration], DESY 08-052 arxiv:0805.4530 Submitted to Phys. Lett. B. and references therein.
8. F.D. Aron *et al.* [H1 Collaboration], DESY 08-009 arxiv:0802.1858 *Phys. Lett.* B **663**, 382 (2008). and references therein.
9. H1 Collaboration, Contributed paper to EPS07 H1prelim-07-163 and references therein.
10. ZEUS Collaboration, Contributed paper to LP07 ZEUS-prel-07-28 and references therein.
11. N. Arkani-Hamed, S. Dimopoulos and G.Dvali, *Phys. Lett.* B **429**, 263 (1998).
12. I. Antioniadis et al., *Phys. Lett.* B **436**, 257 (1998).
13. N. Arkani-Hamed, S. Dimopoulos and G.Dvali, *Phys. Rev.* D **59**, 086004 (1999).
14. G. F. Giudice, R. Rattazzi and J. D. Wells, *Nucl. Phys.* B **544**, 3 (1999).
15. H1 Collaboration, Contributed paper to LP07 H1prelim-07-141 and references therein.

Theoretical issues and methods

Is $N = 8$ Supergravity an Ultraviolet Finite Quantum Field Theory?

K.S. Stelle
Max-Planck Institute for Gravitational Physics
(Albert-Einstein Institute)
Am Mühlenberg 1
D-14476 Potsdam-Golm, Germany

and

Theoretical Physics Group
Imperial College London
Prince Consort Road
London SW7 2AZ, UK

Advances in the computation of quantum amplitudes in supergravity theories raise the question whether maximal supergravity in $D = 4$ spacetime dimensions might actually be free of ultraviolet divergences. On the other hand, supersymmetric non-renormalization theorems give no indication of cancellations for anything beyond half-BPS counterterm operators. The jury is still out, and bets are being taken on the outcome.

Formulating an acceptable quantum theory of gravity remains the prime challenge to fu mental theoretical physics. A basic problem in formulating such a theory was already recogn in the earliest approaches to the problem in the 1930's: the dimensional character of Newt constant gives rise to ultraviolet divergent quantum correction integrals. In the 1970's, this confirmed explicitly in the first Feynman diagram calculations of the radiative corrections to tems containing gravity plus matter [1]. The time lag between the general perception of the divergence problem and its first concrete demonstration was due to the complexity of Feyn diagram calculations involving gravity. The necessary techniques were an outgrowth of the struggle to Lorentz-covariantly control the quantization of non-abelian Yang-Mills theorie the Standard Model of weak and electromagnetic interactions and in quantum chromodynan

With the advent of supergravity [2] in the mid 1970's, hopes rose that the specific combinations of quantum fields in supergravity theories might possibly tame the gravitational UV divergence problem. Indeed, it turns out that all irreducible supergravity theories in four-dimensional spacetime, *i.e.* theories in which all fields are irreducibly linked to gravity by supersymmetry transformations, have remarkable cancellations in Feynman diagrams with one or two internal loops.

There is a sequence of such irreducible (or "pure") supergravity models, characterized by the number N of local (*i.e.* spacetime-dependent) spinor parameters. In four-dimensional spacetime, minimal, or $N = 1$, supergravity thus has 4 supersymmetries corresponding to the components of a single Majorana spinor transformation parameter. The maximal possible supergravity [3] in four dimensional spacetime has $N = 8$ spinor parameters, *i.e.* 32 independent supersymmetries.

The hopes for "miraculous" UV divergence cancellations in supergravity were subsequently dampened by the realization that the divergence-killing powers of supersymmetry most likely do not extend beyond the two-loop order for generic pure supergravity theories [4,5,6,7]. The three-loop anticipated invariant is quartic in curvatures, and has a purely gravitational part given by the square of the Bel-Robinson tensor [4].

The flowering of superstring theory in the 1980's and 1990's, in which the UV divergence problems of gravity are cured by a completely different mechanism replacing the basic field-theory point-particle states by extended relativistic object states, pushed the UV divergence properties of supergravity out of the limelight, leaving the supergravity UV problem in an unclear state.

Nonetheless, among some researchers a faint hope persisted that at least the maximal $N = 8$ supergravity might have special UV properties. This hope was bolstered by the fact that the fact that the maximal supersymmetric Yang-Mills theory, which has $N = 4$, *i.e.* 16-component supersymmetry, is completely free of ultraviolet divergences in four-dimensional spacetime [8]. This was the first interacting UV-finite theory in four spacetime dimensions.

It is this possibility of "miraculous" UV divergence cancellations in maximal supergravity that has now been confirmed in a remarkable 3-loop calculation by Z. Bern et al. [9]. Performing such calculations at high loop orders requires a departure from textbook Feynman-diagram methods, because the standard approaches can produce astronomical numbers of terms. Instead of following the standard propagator & vertex methods for the supergravity calculations, Bern et al. used another technique which goes back to Feynman: loop calculations can be performed using the unitarity properties of the quantum S-matrix. These involve cutting rules that reduce higher-loop diagrams to sums of products of leading-order "tree" diagrams without internal loops. This use of unitarity is an outgrowth of the optical theorem in quantum mechanics for the imaginary part of the S-matrix.

In order to obtain information about the real part of the S-matrix, an additional necessary element in the unitarity-based technique is the use of dimensional regularization to render UV divergent diagrams finite. In dimensional regularization, the dimensionality of spacetime is changed from 4 to $4 - \epsilon$, where ϵ is a small adjustable parameter. Traditional Feynman diagram calculations also often use dimensional regularization, but normally one just focuses on the leading $1/\epsilon$ poles in order to carry out a renormalization program. In the unitarity-based approach, all orders in ϵ need to be retained. This gives rise to logarithms in which real and imaginary contributions are related.

In the maximal $N = 8$ supergravity theory, the complexity of the quantum amplitudes factorizes, with details involving the various field types occurring on the external legs of an amplitude multiplying a much simpler set of scalar-field Feynman diagrams. It is to the latter that the unitarity-based methods may be applied. Earlier applications [10] of the cutting-rule unitarity methods based on iterations of two-particle cuts gave an expectation that one might have cancellations for $D < 10/L + 2$, where D is the spacetime dimension and L is the number

of Feynman diagram loops (for $L > 1$). Already, this gave an expectation that $D = 4$ maximal supergravity would have cancellations of the UV divergences at the $L = 3$ and $L = 4$ loop orders. This would leave the next significant test at $L = 5$ loops. In the ordinary Feynman-diagram approach, a full calculation at this level would involve something like 10^{30} terms. Even using the unitarity-based methods, such a calculation would be a daunting, but perhaps not impossible, task.

The impressive new elements in the 3-loop calculation of Bern et alàre the completeness of their calculation and the unexpected further patterns of cancellations found. This could suggest a possibility of unexpected UV cancellations at yet higher loop orders. Although the various 3-loop diagram classes were already individually expected to be finite on the basis of the earlier work by Bern et al., the new results show that the remaining finite amplitudes display additional cancellations, rendering them "superfinite". In particular, the earlier work employed iterated 2-particle cuts and did not consider all diagram types. The new complete calculation displays further cancellations between diagrams that can be analyzed using iterated 2-particle cuts and the additional diagrams that cannot be treated in this way. The set of three-loop diagrams is shown in Figure 1. The end result is that the sum of all diagram types is more convergent by two powers of external momentum than might otherwise have been anticipated.

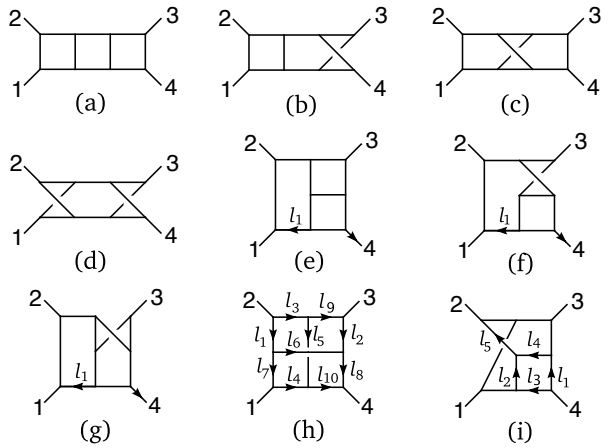

Figure 1: 3-loop Feynman diagram types leading to unanticipated 'superfiniteness' of maximal supergravity at this loop order. Diagrams (a)-(g) can be analyzed using iterated 2-particle cuts, leading to an expectation of ultraviolet divergence cancellation. Diagrams (h) and (i) cannot be treated this way, but the result of summing all diagrams (a-i) is a deeper cancellation of the leading UV behavior than anticipated.

Does such a mechanism cascade in higher-order diagrams, rendering the maximal N=8 theory completely free of ultraviolet divergences? No one knows at present. Such a scenario might pose puzzling questions for the superstring program, where it has been assumed that ordinary supergravity theories need string ultraviolet completions in order to form consistent quantum theories. On the other hand, there are hints [11] from superstring theory that precisely such an all-orders divergence cancellation might take place in the $N = 8$ theory. On the other hand, it is not clear exactly what one can learn from superstring theory about purely perturbative field-theory divergences.

One thing that seems clear is that ordinary Feynman diagram techniques coupled with the "non-renormalization" theorems of supersymmetry are unlikely to be able to explain finiteness properties of $N = 8$ supergravity at arbitrary loop order. Earlier expectations [4,5,6,7] were that the first loop order at which divergences that cannot be removed by field redefinitions would be three loops in all pure $D = 4$ supergravities. A key element in this anticipation was the expectation that the maximal amount of supersymmetry that can be *linearly* realized in Feynman diagram calculations (aka "off-shell supersymmetry") is half the full supersymmetry of the theory, or 16

out of 32 supercharges for the maximal $N = 8$ theory.

Similarly to the way in which chiral integrals of $N = 1$, $D = 4$ supersymmetry achieve invariance from integrals over less than the theory's full superspace, provided the integrand satisfies a corresponding BPS type constraint, there are analogous invariants involving integration over varying portions of an extended supersymmetric theory's full superspace [6]. "Half-BPS" operators require integration over just half the full set of fermionic variables. And if half the full supersymmetry were the maximal amount that can be linearly realized (so giving strong results from the corresponding Ward identities), such operators would be the first to be allowed as UV counterterms.

The results of Ref. [9] show that the half-BPS expectation for the first allowed counterterms is too conservative in the case the maximal theory. But more recent advances in the understanding of supersymmetric non-renormalization theorems push the divergence onset boundary out slightly for the maximal theory, so that half-BPS counterterms that require superspace integrals over half the 32 component superspace are now expected to be the last *disallowed* counterterms instead of the first *allowed* ones. The resulting current expectations for first divergences from a traditional Feynman diagram plus non-renormalization viewpoint are shown for various spacetime dimensions in Table 1.

Dimension D	11	10	8	7	6	5	4
Loop order L	2	2	1	2	3	4	5
Gen. form	$\partial^{12}R^4$	$\partial^{10}R^4$	R^4	∂^6R^4	∂^6R^4	∂^6R^4	∂^4R^4

Table 1: Current maximal supergravity divergence expectations from Feynman rules and non-renormalization theorems.

The behavior of maximal $N = 4$ supersymmetric Yang-Mills theory in dimensions $D > 4$ may be a model for what is happening. Contrary to earlier expectations of UV divergences at the 4 loop order in $D = 5$ spacetime, the unitarity-based methods indicate that this SYM onset should be postponed to the 6-loop order. But here, the standard Feynman diagram methods have a comeback through the realization that the 4-loop finiteness could be explained using more sophisticated "harmonic superspace" methods.[12]

There are two new recent elements to the non-renormalization theorem perspective. One is the realization that maximal SYM can be formulated in a "1/2 SUSY + 1" formalism which is not however Lorentz covariant [13]. Such a SYM formulation dimensionally reduces to (8,1) supersymmetry in $D = 2$. Although considerations of gauge invariance implications in various dimensions are still ongoing, this formulation should be just the minimum needed to rule out the half-BPS operators. Moreover, there is an analogous "1/2 SUSY + 1" formulation for maximal supergravity dimensionally reduced to $D = 2$, having (16,1) supersymmetry. Providing this can be successfully lifted to a viable quantization formalism in $D = 4$, it should be just enough to rule out the $D = 4$ 3-loop candidate counterterm, now known from Ref. [10] not to occur [14].

The second new approach to the derivation of non-renormalization theorems is via "algebraic renormalization", which uses BRST cohomological techniques and has been used to give yet another demonstration of the finiteness of $D = 4$, $N = 4$ SYM [15]. Similar techniques for maximal supergravity are anticipated also to kill the eligibility of the 1/2 BPS $D = 4$ 3-loop candidate counterterm.

The overall picture that emerges from the non-renormalization theorems and the currently known divergence results from calculation is that the half-BPS operators are ruled out as UV counterterms, but that operators with less than half BPS character (thus requiring superspace integrals with more than half of the theory's full supersymmetry) are not. The most accessible test of this proposition will occur at 4 loops in $D = 5$. As is not uncommon in this subject, bets are being taken on the outcome, the payoff to be made in bottles of wine.

References

1. G. 't Hooft and M. Veltman, Annales Inst. Henri Poincare, Section A XX (1974) 69-94.
2. D.Z. Freedman, P. van Nieuwenhuizen and S. Ferrara, Phys. Rev. **D13** (1976) 3214-3218. S. Deser and B. Zumino, Phys. Lett. **B62** (1976) 335-337.
3. E. Cremmer and B. Julia, Nucl. Phys. **B159** (1979)141-212.
4. S. Deser, J.H. Kay and K.S. Stelle, Phys. Rev. Lett. **38** (1977) 527.
5. R.E. Kallosh, Phys. Lett. **B99** (1981) 122.
6. P.S. Howe, K.S. Stelle and P.K. Townsend, Nucl. Phys. **B191** (1981) 445.
7. P.S. Howe, K.S. Stelle and P.K. Townsend, Nucl. Phys. **B236** (1984) 125.
8. P.S. Howe, K.S. Stelle and P.K. Townsend, Nucl. Phys. **B214** (1983) 519; S. Mandelstam, Nucl. Phys. **B213** (1983) 149; L. Brink, O. Lindgren and B. Nilsson, Phys. Lett. **123B** (1983) 328.
9. Z. Bern et al., Phys. Rev. Lett. 98, (2007) 161303(4).
10. Z. Bern et al., Nucl. Phys. B530 (1998) 401-456.
11. N. Berkovits, http://arxiv.org/hep-th/0609006; M.B. Green, J.G. Russo and P. Vanhove, Phys. Rev. Lett. (in press) http://arxiv.org/hep-th/0611273.
12. A. Galperin, E. Ivanov, S. Kalitzin, V. Ogievetsky and E. Sokatchev, Class. Quantum Grav. 2, 155-166 (1985); F. Delduc and J. McCabe, Class. Quantum Grav. 6, 233-254 (1989); P.S. Howe and K.S. Stelle, Phys. Lett. B554, 190-196 (2003).
13. L. Baulieu, N.J. Berkovits, G. Bossard and A. Martin, Phys. Lett. B **658**, 249 (2008) [arXiv:0705.2002 [hep-th]].
14. G. Bossard, P.S. Howe and K.S. Stelle, work in progress.
15. L. Baulieu, G. Bossard and S.P. Sorella, Nucl. Phys. **B 753** (2006) 252, [hep-th/0605164].

HOLOGRAPHIC TECHNIQUES FOR ASYMPTOTICALLY-FREE GAUGE THEORIES

U. GURSOY[1], E. KIRITSIS[1,2], L. MAZZANTI[1], F. NITTI[1]

[1] *CPHT,Ecole Polytechnique, 91128, Palaiseau, FRANCE, (UMR du CNRS 7644)*
[2] *Department of Physics, University of Crete, 71003 Heraklion, GREECE*

Novel techniques based on holographic ideas are tried on the prototype strongly coupled gauge theory: QCD The ideas are developed and a well motivated phenomenological model (Improved Holographic QCD) is presented and compared to various non-perturbative regimes, both at zero and finite temperature.

1 Introduction

Strongly coupled gauge theories are omnipresent in theoretical physics, and have been forced experimentally upon us with the realization that the strong interactions are best described by an asymptotically free SU(3) gauge theory. The gauge coupling is weak at large energies and perturbation theory is applicable. However it is strong at low energy and almost all realistic observables contain parts that are sensitive to strongly coupled physics.

Beyond QCD, theorists have argued that strongly coupled gauge theories can play an important role in the physics beyond the standard model. We will mention here two such incarnations. The first concerns a strongly coupled gauge theory that is responsible for producing a composite Higgs that will break the electroweak symmetry at lower energies, [1]. Such classes of theories come under the name of 'technicolor" and although their popularity had its ups and downs, they are reanalyzed currently due to the use of novel non-perturbative holographic tools.

The second example concerns strong coupling dynamics that can trigger supersymmetry

breaking in a hidden sector. This supersymmetry breaking is expected to be transferred to the Supersymmetric SM sector either via universal interactions (gravity) or via gauge gauge interactions (gauge mediation). We should also mention that in theories beyond the SM, and especially in string theory vacua, strongly coupled hidden sectors are generic [2] and if their associated scales are in the TeV region they might produce signals at LHC.

Various techniques have been developed to deal with the strong coupling problem of gauge theories. The most straightforward one, is numerical evaluation of the quantities of interest on a computer. This is the lattice approach that has been applied mostly to QCD, with considerable success. The lattice approach after 30 years is a mature discipline that has however its limitations, that basically translate into limitations of computing power. Despite the success of computational approaches, several interesting QCD observables remain out of reach, or cannot be computed to the required accuracy (examples are transport coefficients at finite temperature, relevant for recent heavy ion data from RHIC, or the physics at finite baryon number density and chemical potential)

A different theoretical approach was postulated by 't Hooft in 1974, in order to generate a different perturbative expansion of strongly-coupled gauge theories. This is known as the large-N expansion where N is the number of colors. Although it turned out that it was not possible to calculate even the leading approximation in this expansion for 4d gauge theories, several important properties were uncovered [4]: (a) The perturbative expansion in powers of 1/N has the structure of a string theory with string coupling constant $g_s \sim 1/N$. (b) The gauge invariant QCD bound states, namely glueballs and mesons are non-interacting with O(1) masses, to leading order. Their widths vanish as $1/N^2$ for glueballs and 1/N for mesons. (c) Baryons are heavy, with masses N, and behave as solitonic objects. Theorists have attempted to construct this string theory in four dimensions, but existing experience with string theories did not suggest optimism in this direction.

A new twist to the quest of the string theory underlying a strongly coupled gauge theory came with the realization [5] that for such a gauge theory string should propagate in more than 4 dimensions. In a much more symmetric relative of QCD, namely $\mathcal{N}$=4 superconformal SU(N) gauge theory, the dual string theory turned-out to be a type IIB string propagating in a ten-dimensional spacetime of the form $AdS_5 \times S^5$. In particular the fifth (radial) dimension of AdS_5 provided the holographic dimension that somehow captured the RG scale of the four-dimensional gauge theory that was defined on the AdS_5 boundary. This duality turned out to be a weak-strong coupling duality in the following sense: The gauge theory, that is exactly conformally invariant, has two dimensionless parameters: the number of colors N that we take large, and the 't Hooft coupling $\lambda \equiv g^2_{YM} N$ that we keep fixed in the large-N limit. When $\lambda \ll 1$ one can use perturbation theory, and the relevant leading order diagrams are the planar diagrams. When $\lambda \gg 1$ perturbative techniques are of no use even as $N \to \infty$. On the other hand, the dual string theory is propagating on a manifold with curvature scale $1/\ell^2$, whose relation to the string length ℓ_s involves the 't Hooft coupling: $\ell^2 = \sqrt{\lambda}\, \ell_s^2$. Moreover as the YM gauge coupling constant is given by $g^2_{YM} \sim g_s$, the string coupling constant in the large-N limit is given by $g_s \sim \frac{\lambda}{N}$ and for fixed λ it is $\mathcal{O}(1/N)$. Therefore, at large-N and large 't Hooft coupling, $\lambda \to \infty$, the theory is described by a string that moves on a weakly curved ten-dimensional manifold, and can therefore approximated by the dynamics of its zero modes: the strongly coupled large-N sYM theory is equivalent to type IIB supergravity on the $AdS_5 \times S^5$ background.

Since [5] there has been a flurry of attempts to devise such correspondences for gauge theories with less supersymmetry with the obvious final goal: QCD. Several interesting string duals with a QCD-like low-lying spectrum and confining IR physics were proposed [6]. Although such theories reproduced the qualitative features of IR QCD dynamics, they contain Kaluza-Klein modes, not expected in QCD, with KK masses of the same order as the dynamical scale of the gauge theory. Above this scale, the theories deviate from QCD.

A different and more phenomenological approach was in the meantime developed and is now known as AdS/QCD. The original idea was formulated in [7] and it was successfully applied to the meson sector in [8]. The bulk gravitational background consists of a slice of AdS_5, and a constant dilaton. There is a UV and an IR cutoff. Moreover, the confining IR physics is imposed by boundary conditions at the IR boundary. This approach, although crude, has been partly successful in studying meson physics, despite the fact that the dynamics driving chiral symmetry breaking must be imposed by hand via IR boundary conditions. Its shortcomings however include a glueball spectrum that does not fit well the lattice data, the fact that magnetic quarks are confined instead of screened, and asymptotic Regge trajectories for glueballs and mesons are quadratic instead of linear.

2 Improved Holographic QCD

In [9] an improved holographic phenomenological model for QCD was proposed. It reunited inputs from both gauge theory and string theory while keeping the simplicity of a two-derivative action. It could describe both the region of asymptotic freedom as well as the strong IR dynamics of QCD.

The basic fields of the pure gauge theory (the closed string sector) that are non-trivial in the vacuum solution and describe the pure gauge dynamics, are the 5d metric $g_{\mu\nu}$ (dual to the YM stress tensor), a scalar Φ (the dilaton, dual to $Tr[F^2]$) that controls the 't Hooft coupling λ_t of QCD, and an axion a, that is dual to the QCD instanton density $Tr[F \wedge F]$ and its source represents the θ angle. Quarks can be added to the pure gauge theory by adding $D_4 - \bar{D}_4$ brane pairs in the background gauge theory solution. The $D_4 - \bar{D}_4$ tachyon condensation then induces chiral symmetry breaking, [11,9].

The action for the 5D Einstein-dilaton theory reads,

$$S_5 = M_p^3 N_c^2 \left(- \int d^5x \sqrt{g} \left[R - \frac{4}{3} \frac{(\partial\lambda)^2}{\lambda^2} + V(\lambda) \right] + 2 \int_{\partial M} d^4x \sqrt{h}\ K \right) \tag{1}$$

where M_p is the Planck mass. The second term in the action is the Gibbons-Hawking with K being the extrinsic curvature on the boundary.

The only nontrivial input in the two-derivative action of the graviton and the dilaton is the dilaton potential $V(\lambda)$, where $\lambda = e^{\Phi}$. λ is proportional to the 't Hooft coupling of the gauge theory, $\lambda = \kappa\lambda_t$. The constant of proportionality κ is treated as a parameter to be fitted to data. The potential is directly related to the gauge theory β-function once a holographic definition of energy is chosen. Although the shape of $V(\lambda)$ is not fixed without knowledge of the exact gauge theory β-function, its UV and IR asymptotics can be determined.

In the UV, the input comes from perturbative QCD. We demand asymptotic freedom with logarithmic running. This implies in particular that the asymptotic UV geometry is that of AdS_5 with logarithmic corrections. It requires a (weak-coupling) expansion of $V(\lambda)$ of the form $V(\lambda) = 12/\ell^2(1 + v_1\lambda + v_2\lambda^2 + \cdots)$.

Demanding confinement of the color charges restricts the large-λ asymptotics of $V(\lambda)$. In [9] we focused on potentials such that, as $\lambda \to \infty$, $V(\lambda) \sim \lambda^{\frac{4}{3}} (\log\lambda)^{(\alpha-1)/\alpha}$ where α is a positive parameter. The IR asymptotics of the solution in the Einstein frame are:

$$ds_0^2 \to e^{-C\left(\frac{r}{\ell}\right)^{\alpha}} \left(dr^2 + dx_4^2 \right), \quad \lambda_0 \to e^{3C/2\left(\frac{r}{\ell}\right)^{\alpha}} \left(\frac{r}{\ell} \right)^{\frac{3}{4}(\alpha-1)} \tag{2}$$

where the constant C is related to Λ_{QCD}. Confinement requires $\alpha \geq 1$. The parameter α characterizes the large excitation asymptotics of the glueball spectrum, $m_n \sim n^{\frac{\alpha-1}{\alpha}}$. For linear confinement, we choose $\alpha = 2$.

The parameters of the holographic model a priori are: the Planck mass M_p, which governs the scale of interactions between the glueballs in the theory, the parameters v_i that specify the shape of the potential, the scale Λ that plays the role of Λ_{QCD} and the AdS scale ℓ. The latter is not a physical parameter but only a choice of scale: only $\Lambda\ell$ enters into the computation of physical observables. Before choosing a potential, κ that relates λ and the 't Hooft coupling, is not a parameter as the physics is independent of κ. This is characteristic of the leading order in the large-N_c expansion. Once a potential has been chosen then it is not the case anymore as κ can be calculated by comparing for example to the perturbative QCD β-function. A specific choice for $V(\lambda)$ was made in [9] with the appropriate asymptotic properties, that only depended on the parameter κ, hence fixing all v_i. Finally, κ and Λ are fixed by matching to the lattice data for the first two 0^{++} glueball masses. Once Λ is fixed, all other interesting scales like the effective QCD string tension σ are also fixed.

Glueball masses can be obtained by computing the spectrum of normalizable fluctuations of the metric and dilaton around the background solution. In table 1 we give an overview of the glueball spectrum calculated here and its comparison to the best existing lattice data both for $N = 3$ and $N \to \infty$. In figure 1 we give the almost linear trajectories of the 0^{++} and the 2^{++} states as computed from our model.

3 Finite temperature and deconfinement

We will now turn to the finite temperature dynamics in the pure gauge sector derived from the setup of[9]. We find that this setup describes very well the basic features of large-N_c Yang Mills at finite temperature. It exhibits a first order deconfining phase transition. The equation of state and speed of sound of the high temperature phase are remarkably similar to the corresponding lattice results. Moreover, using the zero temperature potential and without adding any extra parameter, we obtain a value for the critical temperature in very good agreement with the one computed from the lattice, [10].

The deconfinement transition. At finite temperature there exist two distinct types of solutions to the action (1) with AdS asymptotics:

i. The thermal graviton gas, obtained by compactifying the Euclidean time in the zero temperature solution with $\tau \sim \tau + 1/T$:

$$ds^2 = b_0^2(r)\left(dr^2 + d\tau^2 + dx_3^2\right),\ \lambda = \lambda_0(r).$$

This solution exists for all $T \geq 0$ and it corresponds to the confined phase, if the gauge theory at zero T confines.

ii. The black hole (BH) solutions (in Euclidean time) of the form:

$$ds^2 = b^2(r)\left(\frac{dr^2}{f(r)} + f(r)d\tau^2 + dx_3^2\right),\ \lambda = \lambda(r). \tag{3}$$

with $f(0) = 1$. There exists a singularity in the interior at $r = \infty$ that is now hidden by a regular horizon at $r = r_h$ where f vanishes. Such solutions correspond to a deconfined phase.

As we discuss below, in confining theories the BHs exist only above a certain minimum temperature, $T > T_{min}$.

The thermal gas as well as BH solution has two parameters: T and Λ. Near the horizon, $f \to f_h(r_h - r)$ with $4\pi T = f_h$. From Einstein's equations, [10]:

$$4\pi\, T = b^{-3}(r_h)\left(\int_0^{r_h} \frac{du}{b(u)^3}\right)^{-1}. \tag{4}$$

In the large-N_c limit, the physics is dominated by the saddle point with minimum free energy. For a given temperature we must therefore compare the free energies of solutions i. and ii.

We introduce a cutoff boundary at $r/\ell = \epsilon$ in order to regulate the infinite volume. The difference of the two scale factors is given near the boundary as

$$b(\epsilon) - b_0(\epsilon) = \mathcal{C}(T)\epsilon^3 + \cdots \tag{5}$$

By the standard rules of AdS/CFT we can relate $\mathcal{C}(T)$ to the difference of VEVs of the gluon condensate: $\mathcal{C}(T) \propto \langle \mathrm{Tr} F^2 \rangle_T - \langle \mathrm{Tr} F^2 \rangle_0$.

The free energy difference is given by

$$\frac{\mathcal{F}}{M_p^3 N_c^2 V_3} = 12\frac{\mathcal{C}(T)}{\ell} - \pi T b^3(r_h) = 12\frac{\mathcal{C}(T)}{\ell} - \frac{TS}{4M_p^3 N_c^2 V_3}, \tag{6}$$

where, in the last equality, we used the fact that the entropy is given by the area of the horizon. It is clear that the existence of a non-trivial deconfinement phase transition is driven by a non-zero value for the thermal gluon condensate $\mathcal{C}(T)$.

For a general potential we can prove the following (under mild assumptions):

i. *There exists a phase transition at finite T, if and only if the zero-T theory confines.*

ii. *This transition is of the first order for all of the confining geometries, with a single exception described in iii:*

iii. *In the limit confining geometry $b_0(r) \to \exp(-Cr)$ (as $r \to \infty$), the phase transition is of the second order and happens at $T = 3C/4\pi$.*

iv. *All of the non-confining geometries at zero T are always in the black hole phase at finite T. They exhibit a second order phase transition at $T = 0^+$.*

We illustrate the function $T(r_h)$ schematically in figure 2. It follows that in the confining geometries $\alpha > 1$, for a given $T > T_{min}$, there always exist a big and a small black hole solution. The big BH has positive specific heat hence it is thermodynamically stable, whereas the small BH is unstable. In the borderline confining geometry $\alpha = 1$, there is a single BH solution.

Existence of a $T_c \geq T_{min}$ follows from the physical requirement of positive entropy. From the first law of thermodynamics, it follows that $d\mathcal{F}/dr_h = -S\, dT/dr_h$. Since $S > 0$ for any physical system, extrema of $\mathcal{F}(r_h)$ coincide with the extrema of $T(r_h)$. Using also the fact that $\mathcal{F}(r_h) \to -\infty$ for $r_h \to 0$ and $\mathcal{F}(r_h) \to 0$ near $r_h \to \infty$, we arrive at conclusion (ii) described above: *There is a first order transition for all of the confining geometries* (This becomes second order for the borderline case $\alpha = 1$).

The small r_h asymptotics also allows us to fix the value of the Planck mass in (1). This geometry corresponds to an ideal gas of gluons with a free energy density (We use lowercase letters for the densities of the corresponding functions) $f \to (\pi^2/45)N_c^2 T^4$. As the geometry becomes AdS, eq. (6) implies that: $f \to \pi^4 (M_p \ell)^3 N_c^2 T^4$. We conclude that $M_p \ell = (45\pi^2)^{-\frac{1}{3}}$. Using the value of ℓ in [9], we obtain $M_p \approx 2.3$ GeV.

4 Numerical Results at finite temperature

In [9] an explicit form of the scalar potential with the correct asymptotics was proposed. The resulting background, that corresponds to the choice $\alpha = 2$ in (2), exhibits asymptotic freedom, linear confinement, and a glueball spectrum in very good quantitative agreement with the lattice data. Here we present a numerical computation of the relevant thermodynamic quantities in this same theory. Our general analysis shows that this theory has black hole solutions above a temperature T_{min} and exhibits a first order phase transition at some $T_c > T_{min}$

To analyze the behavior of the theory at finite temperature, we have solved numerically Einstein's equations for the metric and dilaton. The integration constants were fixed as explained

earlier. We find a minimum temperature for the existence of black hole solutions, $T_{min} = 210$ MeV.

Next, we compute the free energy difference between the black hole and thermal gas solutions, as a function of temperature.

The resulting free energy as a function of the temperature is shown in the left of figure 3, which clearly shows the existence of a minimum temperature, and a first order phase transition at $T = T_c$, where $\mathcal{F}(T_c) = 0$. For $T < T_c$, the thermal gas dominates, and the system is in the confined phase. For $T > T_c$, the (large) black hole dominates, corresponding to a deconfined phase. The entire small black hole branch is always thermodynamically disfavored.

The value we obtain for the critical temperature, $T_c = \mathbf{235 \pm 15}$ MeV, is close to the value obtained for large-N Yang-Mills [12], which with our normalization of the lightest glueball would be 260 ± 11 MeV (combining the results in [12] and [13]).

From the free energy we can determine all other quantities by thermodynamic identities:

$$p = -\mathcal{F}/V_3, \quad s = 4\pi M_p^3 N_c^2 b_T^3(r_h), \quad \epsilon = p + Ts. \tag{7}$$

Next, we present some of the thermodynamic quantities that are compared with the lattice results.

`Latent Heat`. The latent heat per unit volume is defined as the jump in the energy at the phase transition, $L_h = T_c \Delta s(T_c)$, and it is expected to scale as N_c^2 in the large N_c limit [12]. From eq. (7) we note that this expectation is reproduced in our theory. Quantitatively, we find $L_h^{1/4}/T_c \simeq 0.65\sqrt{N_c}$. This is to be compared with the value 0.77 reported in [12].

`Equation of state and the trace anomaly.` A useful indication about the thermodynamics of a system is given by the relations between the quantities ϵ/T^4, $3(p/T^4)$, $3/4(s/T^3)$. In the right of figure 3 we compare our results for these quantities with the corresponding lattice results, reported in [14] (for N_c=3). We find good qualitative agreement. In the low temperature phase, the thermodynamic functions vanish to the leading order in N_c^2 and the jump in ϵ and s at T_c reflects the first order phase transition. The fact that our curves lay below the lattice curves may be traced back to the relative smallness of the latent heat in our model.

The *trace anomaly*, $(\epsilon - 3p)/T^4$, is plotted in the left of figure 4, together with the lattice result from [14]. From eq. (6), $\epsilon - 3p \propto \mathcal{C}(T)$, consistent with our interpretation of $\mathcal{C}(T)$ as the gluon condensate.

`Speed of sound.` This quantity is defined as $c_s^2 = (\partial p/\partial \epsilon)_S = s/c_v$. It is expected to be small at the phase transition, and to reach the conformal value $c_s^2 = 1/3$ at high temperatures. In the right of figure 4 we compare our results with the lattice data, finding good agreement.

`Shear viscosity.` In agreement with the general results of [15], the ratio between shear viscosity and entropy density is $\eta/s = (4\pi)^{-1}$.

Acknowledgments

This article is based on the talk presented by E. Kiritsis at this meeting. U. Gursoy and F. Nitti are supported by European Union Individual Marie Curie fellowships MEIF-CT-2006-039962 and -039369. L. Mazzanti is supported by INFN and ICTP fellowships. This work was partly suposrted by ANR grant, ANR-05-BLAN-0079-02, RTN contracts MRTN-CT-2004-005104 and MRTN-CT-2004-503369, CNRS PICS # 2530, 3059 and 3747, and by a European Union Excellence Grant, MEXT-CT-2003-509661.

References

1. S. Dimopoulos and L. Susskind, Nucl. Phys. B **155** (1979) 237.

J^{PC}	[18] (MeV)	This model (MeV)	Mismatch	$N_c \to \infty$ [17]	Mismatch
0^{++}	**1475 (4%)**	**1475**	0	**1475**	0
2^{++}	2150 (5%)	2055	4%	2153 (10%)	5%
0^{-+}	**2250 (4%)**	**2243**	0		
0^{++*}	**2755 (4%)**	**2753**	0	2814 (12%)	2%
2^{++*}	2880 (5%)	2991	4%		
0^{-+*}	3370 (4%)	3288	2%		
0^{++**}	3370 (4%)	3561	5%		
0^{++***}	3990 (5%)	4253	6%		

Table 1: *Comparison between the glueball spectra in Ref. I and in our model. The states we use as input in our fit are marked in bold. The parenthesis in the lattice data indicate the percent accuracy.*

2. P. Anastasopoulos, T. P. T. Dijkstra, E. Kiritsis and A. N. Schellekens, Nucl. Phys. B **759** (2006) 83 [arXiv:hep-th/0605226].
3. G. 't Hooft, *"A planar diagram theory for strong interactions"* Nucl. Phys. B **72** (1974) 461.
4. A. V. Manohar, [ArXiv:hep-ph/9802419].
5. J. M. Maldacena, Adv. Theor. Math. Phys. **2**, 231 (1998) [Int. J. Theor. Phys. **38**, 1113 (1999)]
6. E. Witten, Adv. Theor. Math. Phys. **2** (1998) 505 [ArXiv:hep-th/9803131]; J. M. Maldacena and C. Nunez, Phys. Rev. Lett. **86** (2001) 588 [ArXiv:hep-th/0008001]; I. R. Klebanov and M. J. Strassler, JHEP **0008** (2000) 052 [ArXiv:hep-th/0007191].
7. J. Polchinski and M. J. Strassler, Phys. Rev. Lett. **88** (2002) 031601 [ArXiv:hep-th/0109174]; Phys. Rev. Lett. **88** (2002) 031601 [ArXiv:hep-th/0109174].
8. J. Erlich, E. Katz, D. T. Son and M. A. Stephanov, Phys. Rev. Lett. **95**, 261602 (2005) [arXiv:hep-ph/0501128]; L. Da Rold and A. Pomarol, Nucl. Phys. B **721**, 79 (2005) [ArXiv:hep-ph/0501218].
9. U. Gursoy and E. Kiritsis, JHEP **0802** (2008) 032 [arXiv:0707.1324 [hep-th]]; U. Gursoy, E. Kiritsis and F. Nitti, JHEP **0802** (2008) 019 [arXiv:0707.1349 [hep-th]].
10. U. Gursoy, E. Kiritsis, L. Mazzanti and F. Nitti, arXiv:0804.0899 [hep-th].
11. R. Casero, E. Kiritsis and A. Paredes, Nucl. Phys. B **787** (2007) 98; [ArXiv:hep-th/0702155].
12. B. Lucini, M. Teper and U. Wenger, JHEP **0502**, 033 (2005) [arXiv:hep-lat/0502003].
13. B. Lucini and M. Teper, JHEP **0106**, 050 (2001) [arXiv:hep-lat/0103027].
14. G. Boyd, J. Engels, F. Karsch, E. Laermann, C. Legeland, M. Lutgemeier and B. Petersson, Nucl. Phys. B **469**, 419 (1996) [arXiv:hep-lat/9602007].
15. A. Buchel and J. T. Liu, Phys. Rev. Lett. **93**, 090602 (2004) [arXiv:hep-th/0311175].
16. S. S. Gubser and A. Nellore, arXiv:0804.0434 [hep-th].
17. B. Lucini and M. Teper, *"SU(N) gauge theories in four dimensions: Exploring the approach to N =∞,"* JHEP **0106** (2001) 050 [ArXiv:hep-lat/0103027].
18. H. B. Meyer, *"Glueball Regge trajectories,"* [ArXiv:hep-lat/0508002].

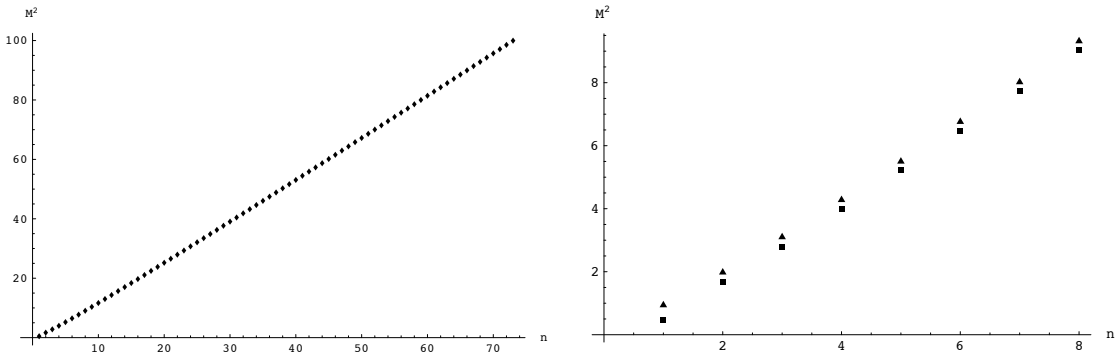

Figure 1: *Left: Linear pattern in the spectrum for the first 40* 0^{++} *glueball states.* M^2 *is shown units of* $0.015\ell^{-2}$. *Right: The first 8* 0^{++} *(squares) and the* 2^{++} *(triangles) glueballs. We used* $b_0 = 4.2, \lambda_0 = 0.05$.

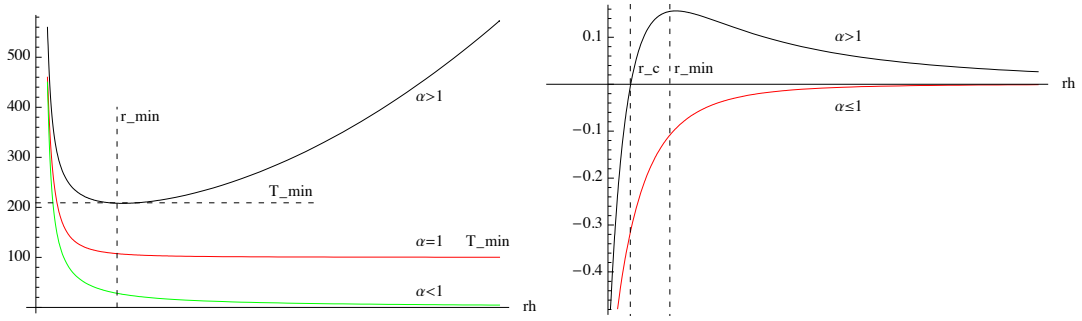

Figure 2: Schematic behavior of temperature as a function of r_h (left) and the free energy density as a function of r_h, (right) for the infinite-r geometries of the type (2), for different values of α.

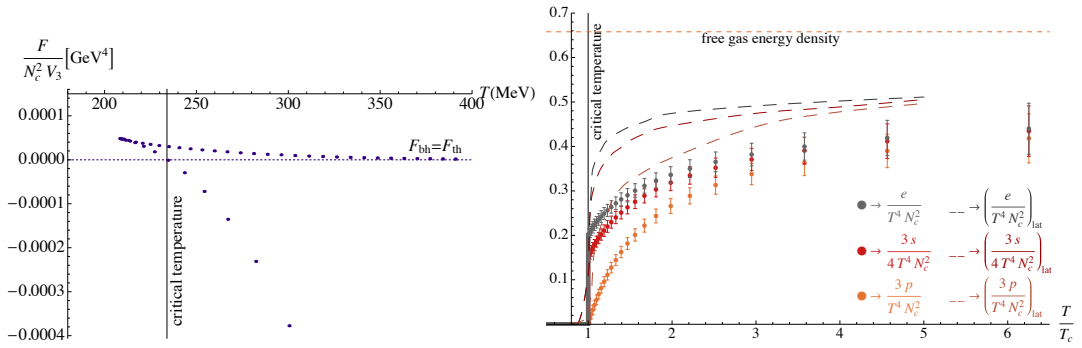

Figure 3: Left: Black hole free energy. Right: Dimensionless thermodynamic functions. The dashed curves correspond to the lattice data of reference [14].

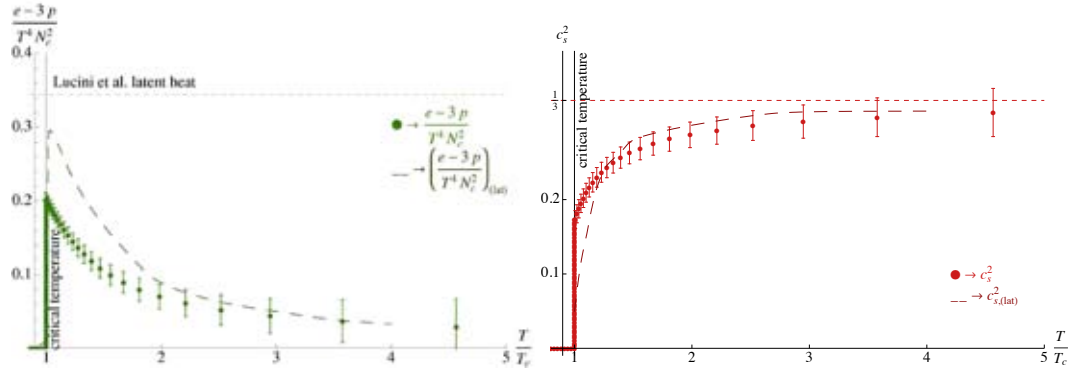

Figure 4: *Left: The trace anomaly. Right: The speed of sound. The dashed curves are the lattice result of reference [14].*